Inorg. Chem. **2009**, *48*, 4118−4133

Properties of the $[M(dppm)_2M']^{2+}$ Building Blocks (M, M′ = Pd or Pt): Site Selectivity, Emission Features, and Frontier Orbital Analysis

Sébastien Clément,[†] Shawkat M. Aly,[‡] Diana Bellows,[‡] Daniel Fortin,[‡] Carsten Strohmann,[§] Laurent Guyard,[†] Alaa S. Abd-El-Aziz,[||] Michael Knorr,*[,†] and Pierre D. Harvey*[,‡]

Institut UTINAM UMR CNRS 6213, Université de Franche-Comté, 16 route de Gray, 25030 Besançon, France, Département de Chimie, Université de Sherbrooke, Sherbrooke, PQ, Canada, J1K 2R1, Technische Universität Dortmund, Anorganische Chemie Otto-Hahn-Str. 6, D-44227 Dortmund, Germany, and Department of Chemistry, University of British Columbia Okanagan, Kelowa, BC, Canada

Received December 5, 2008

The homodinuclear [ClM(μ-dppm)$_2$MCl] complexes **1** (M = Pd) and **2** (M = Pt) react with RNC ligands (R = Ph, xylyl, *p*-tolyl, *p*-C_6H_4*i*Pr) to provide the A-frame [ClPd(μ-dppm)$_2$(μ-C═N−R)PdCl] (R = Ph (**5a**), xylyl (**5b**)), [ClPt(μ-dppm)$_2$(μ-C═N−R)PtCl] (R = *p*-tolyl (**4a**); *p*-C_6H_4*i*Pr (**4b**)), and the d^9−d^9 M_2-bonded [ClPt(μ-dppm)$_2$Pt(CN−R)]Cl (R = xylyl (**3a**); *p*-C_6H_4*i*Pr (**3b**)) complexes. The heterodinuclear [XPd(μ-dppm)$_2$PtX] complexes **6a** (X = Cl) and **6b** (X = I) react with RNC (R = *o*-anisyl) to form the A-frame [XPd(μ-dppm)$_2$(μ-C═N−R)PtX] (X = Cl (**9**); I (**10a**)) and M_2-bonded [ClPt(μ-dppm)$_2$Pt(CN−R)]Cl (**10b**) complexes. The dangling ligand-containing complex [ClPd(μ-dppm)$_2$Pt(η^1-dppm═O)](BF_4) (**7**) reacts with xylyl-NC stoichiometrically to produce the dicationic salt [(xylyl-NC)Pd(μ-dppm)$_2$Pt(η^1-dppm═O)](BF_4)$_2$ (**8**). Parameters ruling the coordination site terminal versus bridging are discussed. The precursor **10a** reacts with RNC (R = *o*-anisyl, *t*Bu) to form the heterobimetallic bis(isonitrile) [IPd(μ-dppm)$_2$(μ-C═N-*o*-anisyl)Pt(CN−R)]I complexes **11b** and **12**, respectively, demonstrating the site selectivity of the second CNR ligand coordination, Pd versus Pt. The X-ray structures of **11b** and **12** were obtained. Complex **12** is the first example of an A-frame system of the Ni-triad bearing two different isocyanide ligands. Several d^9−d^9 terminal and d^8−d^8 A-frame homo- and heterodinuclear complexes in 2-MeTHF at 77 K were studied by UV−vis and luminescence spectroscopy. Assignments for the lowest energy absorption and emission bands are made on the basis of density functional theory and time-dependent density functional theory computations.

Introduction

The M-containing macromolecules and polymers have gained tremendous interest recently for their potential applications in photonics and advanced materials.[1] Among the transition metals, one finds Pd and Pt occupying a major place in this wide family,[2,3] but very few works concerning M−M bond-containing oligomers and polymers.[4] Recently, one of us (P.D.H.) investigated in detail the physical properties of conjugated and nonconjugated Pd−Pd and Pt−Pt bond-containing coordination and organometallic polymers in the solid state and in solution (Chart 1).[5] Evidence for electronic communication along the polymer backbone in the conjugated polymers was provided.

Concurrently, the electron-rich Pd−Pd and Pt−Pt bonds, formally called d^9−d^9, are capable of oxidatively adding two-electron donor substrates to form A-frame d^8−d^8 species

* To whom correspondence should be addressed. E-mail: michael.knorr@univ-fcomte.fr (M.K.); pierre.harvey@usherbrooke.ca (P.D.H.).
[†] Université de Franche-Comté.
[‡] Université de Sherbrooke.
[§] Technische Universität Dortmund.
[||] University of British Columbia at Okanagan.

(1) (a) Abd-El-Aziz, A. S.; Carraher, C. E., Jr.; Pittman, C. U., Jr.; Sheats, J. E.; Zeldin, M. *Macromolecule Containing Metal and Metal-like Elements*; Wiley Interscience, John Wiley and Sons Inc.: New York, 2005; Vol. *5*. (b) *Frontiers in Transition Metal-Containing Polymers*; Abd-El-Aziz, A. S., Manners, I., Eds.; John Wiley and Sons: New York, 2007. (c) Manners, I. *Science* **2001**, *294*, 1664–1666. (d) Manners, I. *Synthetic Metal-Containing Polymers*; Wiley-VCH: Weinheim, Germany, 2004. (e) Newkome, G. R.; He, E.; Moorefield, C. N. *Chem. Rev.* **1999**, *99*, 1689–1746. (f) Astruc, D.; Chardac, F. *Chem. Rev.* **2001**, *101*, 2991–3023. (g) Abd-El-Aziz, A. S. *Macromol. Symp.* **2003**, *196*, 1. (h) Abd-El-Aziz, A. S.; Harvey, P. D. *Macromol. Symp.* **2004**, *209*, 1. (i) Wolf, M. O. *Adv. Mater.* **2001**, *13*, 545–553. (j) Archer, R. D. *Inorganic and Organometallic Polymers*; John Wiley & Sons Inc.,: New York, 2001.

10.1021/ic8023315 CCC: $40.75
Published on Web 04/06/2009

Chart 1

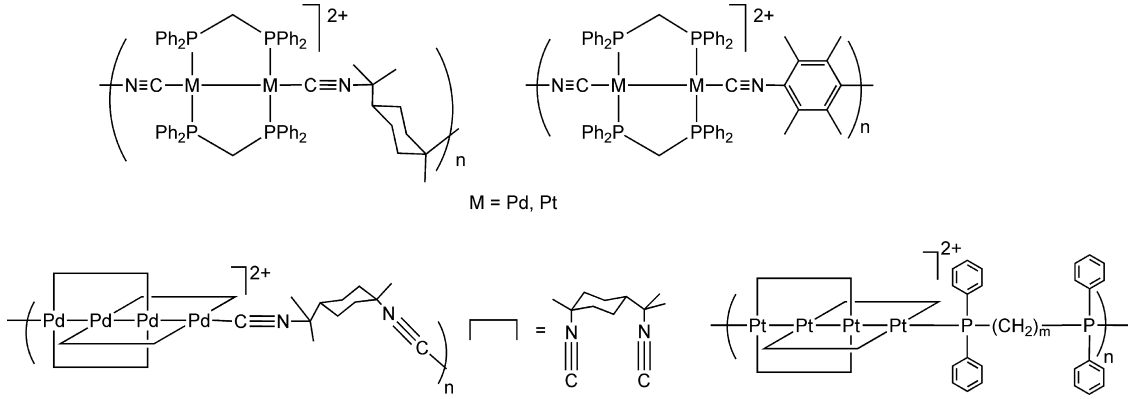

where no M−M bond exists.[6] This feature is extremely interesting since it was recently demonstrated that the electronic communication was completely shut down when the linear conjugated d^9-d^9 complex $Pt_2(dppm)_2(C{\equiv}CFc)_2$ (Fc = ferrocenyl) was reacted with different substrates, including AuCl, to form the corresponding d^8-d^8 A-frame complex.[7] This feature opens the doors for potential applications in photonic materials, such as sensors, where the stimulus is the reversible oxidative addition of a given substrate onto the electron-rich M−M bond being part of a conjugated backbone of a polymer. In principle, because the conjugated polymer is long in comparison with a single dinuclear complex, the amount of substrate does not need to be large to affect the overall physical, optical, and photophysical properties of the materials.

We now wish to report the chemical and structural properties of a series of homo- and hetero-M−M bonded complexes, as well as A-frame dimers, notably with respect to site selectivity in heterobimetallic systems, and to their photophysical behavior in comparison with other related dinuclear compounds. A full understanding on what controls terminal versus bridging coordination properties for various CNR donors is crucial for the structural design of P- and CNR-containing organometallic and coordination polymers. The heterobimetallic systems are particularly interesting because of the potential in building "head-to-tail" polymers by making judicious choices of mixed-donor bidentate ligands.

Experimental Section

Materials. All reactions were performed in Schlenk-tube flasks under purified nitrogen. Compounds ClPd(μ-dppm)$_2$PdCl (**1**), ClPt(μ-dppm)$_2$PtCl (**2**), ClPd(μ-dppm)$_2$PtCl (**6a**), IPd(μ-dppm)$_2$PtI (**6b**), and [ClPd(μ-dppm)$_2$Pt(η^1-dppm=O)](BF$_4$) (**7**) were prepared according to literature methods.[8,9,10a] *o*-Anisylisocyanide was prepared according to a procedure similar to one described for *p*-anisylisocyanide.[11] The following materials were purchased from commercial suppliers: xylylisocyanide (Fluka) and *tert*-butylisocyanide (Aldrich). All solvents were dried and distilled from appropriate drying agents.

[ClPt(μ-dppm)$_2$Pt(CNxylyl)](BF$_4$) (3a′). Xylylisocyanide (0.013 g, 0.100 mmol), diluted in 2 mL of CH_2Cl_2, was added over 30 min to a stirred solution of **2** (0.123 g, 0.100 mmol) in 3 mL of CH_2Cl_2. After one day, $NaBF_4$ (0.110 g, 10 equiv) was added, and stirring was continued for one week. After filtration, the volume of the yellowish solution was reduced under a vacuum and layered

(2) Harvey, P. D. In *Frontiers in Transition Metal-Containing Polymers*; Abd-El-Aziz, A., Manners, I., Eds.; Wiley Interscience: New York, 2006; pp 321−368.
(3) Wong, W.-Y. *J. Inorg. Organomet. Polym. Mater.* **2005**, *15*, 197–219.
(4) (a) Fournier, E.; Sicard, S.; Decken, A.; Harvey, P. D. *Inorg. Chem.* **2004**, *43*, 1491–1501. (b) Irwin, M. J.; Jia, G.; Vittal, J. J.; Puddephatt, R. J. *Organometallics* **1996**, *15*, 5321–5329. (c) Sicard, S.; Bérubé, J.-F.; Samar, D.; Messaoudi, A.; Fortin, D.; Lebrun, F.; Fortin, J.-F.; Decken, A.; Harvey, P. D. *Inorg. Chem.* **2004**, *43*, 5321–5334. (d) Tanase, T.; Goto, E.; Begum, R. A.; Hamaguchi, M.; Zhan, S.; Iida, M.; Sakai, K. *Organometallics* **2004**, *23*, 5975–5988. (e) Zhang, T.; Drouin, M.; Harvey, P. D. *Inorg. Chem.* **1999**, *38*, 1305–1315. (f) Zhang, T.; Drouin, M.; Harvey, P. D. *Inorg. Chem.* **1999**, *38*, 957–963. (g) Zhang, T.; Drouin, M.; Harvey, P. D. *Inorg. Chem.* **1999**, *38*, 4928–4936.
(5) Bérubé, J.-F.; Gagnon, K.; Fortin, D.; Decken, A.; Harvey, P. D. *Inorg. Chem.* **2006**, *45*, 2812–2823.
(6) (a) Evrard, D.; Groison, K.; Decken, A.; Mugnier, Y.; Harvey, P. D. *Inorg. Chim. Acta* **2006**, *359*, 2608–2615. (b) Yip, J. H. K.; Wu, J.; Wong, K.-Y.; Ho, K. P.; Koh, L. L.; Vittal, J. J. *Eur. J. Inorg. Chem.* **2004**, *105*, 6–1062. (c) Foch, I.; Besenyei, G.; Simandi, L. I. *Inorg. Chem.* **1999**, *38*, 3944–3946. (d) Kluwe, C.; Müller, J.; Davies, J. A. *J. Organomet. Chem.* **1996**, *526*, 385–387. (e) Besenyei, G.; Parkanyi, L.; Simandi, L.; James, B. R. *Inorg. Chem.* **1995**, *34*, 6118–6123. (f) Toronto, D. V.; Balch, A. L. *Inorg. Chem.* **1994**, *33*, 6132–6139. (g) Neve, F.; Longeri, M.; Ghedini, M.; Crispini, A. *Inorg. Chim. Acta* **1993**, *205*, 15–22. (h) Neve, F.; Ghedini, M.; Tiripicchio, A.; Ugozzoli, F. *Organometallics* **1992**, *11*, 795–801. (i) Uson, R.; Fornies, J.; Navarro, R.; Tomas, M.; Fortuno, C.; Cebollada, J. I.; Welch, A. J. *Polyhedron* **1989**, *8*, 1045–1052. (j) Davies, J. A.; Pinkerton, A. A.; Syed, R.; Vilmer, M. *J. Chem. Soc., Chem. Commun.* **1988**, 47–49. (k) Arsenault, G. J.; Manojlovic-Muir, L.; Muir, K. W.; Puddephatt, R. J.; Treurnicht, I. *Angew. Chem., Int. Ed. Engl.* **1987**, *26*, 86–87. (l) Uson, R.; Fornies, J.; Navarro, R.; Cebollada, J. I. *J. Organomet. Chem.* **1986**, *304*, 381–390. (m) Uson, R.; Fornies, J.; Espinet, P.; Fortuno, C. *Inorg. Chim. Acta* **1984**, *87*, 207–211. (n) Puddephatt, R. J.; Azam, K. A.; Hill, R. H.; Brown, M. P.; Nelson, C. D.; Moulding, R. P.; Seddon, K. R. *J. Am. Chem. Soc.* **1983**, *105*, 5642–5646. (o) Balch, A. L.; Hunt, C. T.; Lee, C.-L.; Olmstead, M. M.; Farr, J. P. *J. Am. Chem. Soc.* **1981**, *103*, 3764–3772. (p) Brown, M. P.; Fischer, J. R.; Puddephat, R. J.; Seddon, K. R. *Inorg. Chem.* **1979**, *18*, 2808–2813.
(7) Yip, J. H.; Wu, J.; Wong, K.-Y.; Ho, K. P.; Pun, C. S.-N.; Vittal, J. J. *Organometallics* **2002**, *21*, 5292–5300.
(8) Grossel, M. C.; Batson, J. R.; Moulding, R. P.; Seddon, K. R. *J. Organomet. Chem.* **1986**, *304*, 391–423.
(9) Pringle, P. G.; Shaw, B. L. *J. Chem. Soc., Dalton Trans.* **1983**, *5*, 889–897.
(10) (a) Evrard, D.; Clément, S.; Lucas, D.; Hanquet, B.; Knorr, M.; Strohmann, C.; Decken, A.; Mugnier, Y.; Harvey, P. D. *Inorg. Chem.* **2006**, *45*, 1305–1315. (b) Clément, S.; Aly, S. M.; Fortin, D.; Guyard, L.; Knorr, M.; Abd-El-Aziz, A. S.; Harvey, P. D. *Inorg. Chem.* **2008**, *47*, 10816–10824.
(11) Wagner, N. L.; Murphy, K. L.; Haworth, D. T.; Bennett, D. W. In *Inorganic Syntheses*; Wiley-VCH: New York, 2004; Vol. *34*, pp 24−29.

with diethyl ether. After several days, yellow needles were formed. Yield: 0.113 g (80%). IR (KBr): 2157 (s) (ν_{CN}) cm^{-1}. ^{1}H NMR ($CDCl_3$): δ 6.76−8.00 (m, 43H, Ph), 4.59 (m, br, 4H, PCH_2P, $^3J_{Pt-H}$ = 60), 1.70 (s, 6H, CH_3) ppm. ^{31}P{^{1}H} NMR ($CDCl_3$): δ 1.2 (m, 2P, $^1J_{Pt-P}$ = 2370, N = 90), −1.7 (m, 2P, $^1J_{Pt-P}$ = 3070, N = 90). UV−vis (CH_2Cl_2) (λ_{max} nm (ε)): 226 (62700), 348 (4500). Anal. calcd for $C_{59}H_{53}BClNF_4P_4Pt_2\cdot CH_2Cl_2$: C, 48.12; H, 3.67. Found: C, 47.88; H, 3.55.

[ClPt(μ-dppm)$_2$(μ-C=N−C$_6$H$_4$−*i*Pr)PtCl] (4b) and [ClPt(μ-dppm)$_2$Pt(CN−C$_6$H$_4$−*i*Pr)]Cl (3b). 1-Isocyano-4-isopropylbenzene (0.039 g, 0.268 mmol) in 2 mL of CH_2Cl_2 was added to a stirred solution of **2** (0.330 g, 0.268 mmol) in 10 mL of CH_2Cl_2 over a period of 30 min. The orange solution was stirred for 1 h and evaporated to dryness. The orange residue was then dissolved in a minimum amount of CH_2Cl_2 and precipitated with hexane, washed with ether (2 × 5 mL), and dried under a vacuum. Yield: 0.270 g (73%). **4b.** IR (KBr): 1616 (w) ($\nu_{C=N}$) cm^{-1}. ^{1}H NMR ($CDCl_3$): δ 6.90−8.10 (m, 44H, Ph), 4.63 (m, br., 4H, PCH_2P, $^3J_{Pt-H}$ = 60), 2.92 (h, 1H, CH(CH$_3$)$_2$, $^3J_{H-H}$ = 6.8), 1.12 (d, 6H, CH(CH_3)$_2$, $^3J_{H-H}$ = 6.8) ppm. ^{31}P{^{1}H} NMR ($CDCl_3$): δ 17.9 (s, 4P, $^1J_{Pt-P}$ = 3480). **3b.** IR (CH_2Cl_2): 2162 (s) (ν_{CN}) cm^{-1}. ^{31}P{^{1}H} NMR ($CDCl_3$): δ 7.5 (m, 2P, $^1J_{Pt-P}$ = 3220), 3.4 (m, 2P, $^1J_{Pt-P}$ = 2980). ^{1}H NMR ($CDCl_3$): δ 6.55−8.10 (m, 44H, Ph), 3.83 (m, br, 4H, PCH_2P, $^3J_{Pt-H}$ = 60.2), 2.59 (h, 1H, CH(CH$_3$)$_2$, $^3J_{H-H}$ = 7.4), 1.09 (d, 6H, CH(CH_3)$_2$, $^3J_{H-H}$ = 7.4) ppm. Anal. calcd for $C_{60}H_{55}Cl_2NP_4Pt_2\cdot 0.5\ CH_2Cl_2$: C, 51.27; H, 3.95; N, 0.99. Found: C, 51.14; H, 3.82; N, 0.95.

[(xylylNC)Pd(μ-dppm)$_2$Pt(η^1-dppm=O)](BF$_4$)$_2$ (8). Xylylisocyanide (0.011 g, 0.084 mmol), diluted in 1 mL of CH_2Cl_2, was added within 30 min to a stirred solution of **7** (0.120 g, 0.076 mmol) in 2 mL of CH_2Cl_2. After one day, $NaBF_4$ (0.084 g, 10 equivalents) was added, and stirring was continued for one week. The mixture was filtered and evaporated to dryness. The resulting orange residue was washed with diethyl ether and dried. Yield: 0.121 g (90%). IR (KBr): 2167(s) (ν_{CN}) cm^{-1}. ^{1}H NMR ($CDCl_3$): δ 6.99−7.77 (m, 63H, Ph), 6.80 (m, 4H, PCH_2P), 4.56 (m, br, 2H, PCH_2P), 1.76 (s, 6H, CH_3). ^{31}P{^{1}H} NMR ($CDCl_3$): 25.6 (s, Pt−PCH$_2$*P*=O), −0.98 (Pt−*P*(η^1-dppm), $^1J_{Pt-P}$ = 2580, N = 90 Hz), −3.98 (m, Pt−*P*(μ-dppm), $^1J_{Pt-P}$ = 2450, N = 80 Hz), −6.18 (m, Pd−*P*(μ-dppm)). UV−vis (CH_2Cl_2) (λ_{max} nm (ε)): 227 (57500), 270 (22400), 307 (13500), 375 nm (3100). Anal. calcd for $C_{84}H_{75}B_2F_8NOP_6PdPt\cdot 2CH_2Cl_2$: C, 53.05; H, 4.06; N, 0.72. Found: C, 52.98; H, 4.03, N, 0.69.

[ClPd(μ-dppm)$_2$(μ-C=N−C$_6$H$_4$−OCH$_3$)PtCl] (9). *o*-Anisylisocyanide (0.013 g, 0.100 mmol) in 2 mL of CH_2Cl_2 was added slowly over a period of 30 min to a stirred solution of **6a** (0.114 g, 0.100 mmol) in 3 mL of CH_2Cl_2. After 1 h, the yellowish solution was evaporated to dryness. The orange residue was washed with 5 mL of Et_2O and dried under a vacuum. Yield: 0.103 g (81%). IR (KBr): 1616 ($\nu_{C=N}$) cm^{-1}. ^{1}H NMR ($CDCl_3$): δ 5.98−7.78 (m, 44H, Ph), 3.54 (s, 3H, OCH_3), 3.28 (m, br, 2H, PCH_2P), 2.82 (m, br, 2H, PCH_2P). ^{31}P{^{1}H} NMR ($CDCl_3$): δ 12.1 (m, 4P, $^1J_{Pt-P}$ = 3560, $^3J_{Pt-P}$ = 495). UV−vis (MeCN) (λ_{max} nm (ε)): 227 (51800), 267 (18900), 348 (2700). Anal. calcd for $C_{58}H_{51}Cl_2NOP_4PdPt$: C, 54.67; H, 4.03; N, 1.10. Found: C, 54.49; H, 4.42; N, 1.00.

[IPd(μ-dppm)$_2$Pt(CN−C$_6$H$_4$−OCH$_3$)]I (10b) and [IPd(μ-dppm)$_2$Pt(μ-C=N−C$_6$H$_4$−OCH$_3$)I] (10a). *o*-Anisylisocyanide (0.013 g, 0.100 mmol) in 2 mL of CH_2Cl_2 was added to a stirred solution of **6b** (0.132 g, 0.100 mmol) in 3 mL of CH_2Cl_2 over a period of 30 min. The reddish solution was stirred for 1 h and evaporated to dryness. The orange residue was washed with 5 mL of Et_2O and dried in a vacuum. Yield: 0.125 g (86%). **10b.** IR (CH_2Cl_2/MeOH): 2175 cm^{-1} (ν_{CN}). ^{31}P{^{1}H} NMR ($CDCl_3$/MeOH): δ −8.9 (m, 2P, Pd−*P*, $^{2+3}J_{Pt-P}$ = 52), −3.1 (m, 2P, Pt−*P*, $^1J_{Pt-P}$ = 2590, N = 80 Hz). ^{195}Pt{^{1}H} NMR ($CDCl_3$/MeOH): δ −2758 (tt, $^1J_{Pt-P}$ = 2590, $^{2+3}J_{Pt-P}$ = 50). **10a.** IR (KBr): 1611 cm^{-1} ($\nu_{C=N}$). ^{1}H NMR ($CDCl_3$): δ 3.53 (s, 3H, OCH_3), 4.77 (t, 4H, PCH$_2$P), 6.99−7.77 (m, 44H, Ph). ^{31}P{^{1}H} NMR ($CDCl_3$): δ 10.8 (t, 2P, Pt−*P*, $^1J_{Pt-P}$ = 3465, N = 75 Hz), 12.3 (t, 2P, Pd−*P*, $^3J_{Pt-P}$ = 520). Anal. calcd for $C_{58}H_{51}I_2NOP_4PdPt$: C, 47.80; H, 3.53; N 1.05. Found: C, 47.56; H, 3.53; N, 0.96.

[XPd(μ-dppm)$_2$(μ-C=N−C$_6$H$_4$-2-OCH$_3$)Pt(CN−C$_6$H$_4$-2-OCH$_3$)]X (11a, X = Cl; 11b, X = I). *o*-Anisylisocyanide (0.027 g, 0.200 mmol), diluted in 2 mL of CH_2Cl_2, was added over a period of 30 min to a stirred solution of **6a** or **6b** (0.100 mmol) in 3 mL of CH_2Cl_2. After 2 h, the reddish solution was evaporated to dryness. The orange residue was washed with 5 mL of Et_2O and dried under a vacuum. **11a.** Yield: 93% (0.131 g). IR (KBr): 2171 (s) (ν_{CN}), 1621 (w) ($\nu_{C=N}$) cm^{-1}. ^{1}H NMR ($CDCl_3$): δ 5.98−7.95 (m, 48H, Ph), 3.51 (s, 3H, OCH_3), 3.39 (m, br, 4H, PCH_2P), 3.14 (s, 3H, OCH_3). ^{31}P{^{1}H} NMR ($CDCl_3$): δ 16.1 (m, 2P, Pt−*P*(μ-dppm), $^1J_{Pt-P}$ = 3210, N = 80 Hz), 18.3 (m, 2P, Pd-*P*(μ-dppm), $^3J_{Pt-P}$ = 302). ^{195}Pt{^{1}H} NMR ($CDCl_3$): δ −2856 (tt, $^1J_{Pt-P}$ = 3210, $^3J_{Pt-P}$ = 302). UV (MeCN): λ_{max} (ε) = 224 (65800), 289 (36200), 384 (4100), 459 (2050). Anal. Calcd for $C_{66}H_{58}Cl_2N_2O_2P_4PdPt\cdot CH_2Cl_2$: C, 53.92; H, 4.03; N, 1.88, Found: C, 53.69; H, 4.09; N, 1.84. **11b.** Yield: 0.135 g (80%). IR (KBr): 2174 (s) (ν_{CN}), 1630 ($\nu_{C=N}$). ^{1}H NMR ($CDCl_3$, 213 K): δ 6.10−7.90 (m, 48H, Ph), 3.63 (s, 3H, OCH_3), 3.46 (m, br, 4H, PCH_2P), 3.17 (s, 3H, OCH_3). ^{13}C{^{1}H} NMR ($CDCl_3$): 20.3 (2C, P*C*H$_2$P), 55.9 (2C, O*C*H$_3$), 112.0, 120.6 (Ph), 122.2 (2C, *C*N), 128.3−134.6 (Ph), 153 (=*C*−OMe). ^{31}P{^{1}H} NMR ($CDCl_3$): δ 15.0 (m, 2P, Pt−*P*, $^1J_{Pt-P}$ = 3225, N = 85 Hz), 20.8 (m, 2P, Pd-*P*, $^3J_{Pt-P}$ = 300). ^{195}Pt{^{1}H} NMR ($CDCl_3$): δ −2825 (tt, $^1J_{Pt-P}$ = 3225, $^3J_{Pt-P}$ = 300). UV−vis (CH_2Cl_2) (λ_{max} nm (ε)): 245 (54200), 292 (20400), 406 (3560), 450 (4150). Anal. calcd for $C_{66}H_{58}I_2N_2O_2P_4PdPt\cdot 0.5CH_2Cl_2$: C, 48.87; H, 3.61; N 1.71. Found: C, 48.91; H, 3.65; N, 1.72.

[IPd(μ-dppm)$_2$Pt(μ-C=N−C$_6$H$_4$−OCH$_3$)(CN-tBu)]I (12). *Tert*-butylisocyanide (0.008 g, 0.100 mmol) dissolved in 1 mL of CH_2Cl_2 was added to a stirred solution of **9** (0.156 g, 0.100 mmol) in 3 mL of CH_2Cl_2 over a period of 30 min. The orange solution was stirred for 1 h. Its volume was reduced under a vacuum and layered with Et_2O to afford X-ray-suitable orange crystals. Yield: 0.136 g (83%). ^{1}H NMR ($CDCl_3$): δ 6.10−7.90 (m, 44 H, Ph), 3.43 (s, 3H, OCH_3), 3.16 (m, br, 4H, PCH_2P), 0.86 (s, 9H, *tBu*). ^{31}P{^{1}H} NMR ($CDCl_3$): δ 14.9 (m, 2P, Pt−*P*(μ-dppm), $^1J_{Pt-P}$ = 3222, N = 81 Hz), 19.9 (m, 2P, Pd−*P*(μ-dppm), $^3J_{Pt-P}$ = 325). ^{195}Pt{^{1}H} NMR ($CDCl_3$): δ −2860 (tt, $^1J_{Pt-P}$ = 3220, $^3J_{Pt-P}$ = 325). Mass FAB (NBA-matrix) (rel. int.): 1328 (6%) PdPt(dppm)$_2$I(CN−C$_6$H$_4$−OMe), 1196 (100%) PdPt(dppm)$_2$I, 1068.0 (40%) PdPt(dppm)$_2$. Anal. calcd for $C_{63}H_{60}I_2N_2OP_4PdPt$: C, 49.12; H, 3.92; N, 1.82. Found: C, 49.06; H, 4.15; N, 1.83.

Apparatus. IR spectra have been recorded on a Nicolet Nexus 470 spectrometer. All NMR spectra were acquired with a Bruker Avance 300 (^{1}H 300.13 MHz, ^{13}C 75.48 MHz and ^{31}P 121.49 MHz) using the solvent as the chemical shift standard, except for ^{31}P NMR, where the chemical shifts are relative to 85% H_3PO_4 in D_2O. ^{195}Pt chemical shifts were measured on a Bruker ACP 200 instrument (42.95 MHz) and externally referenced to K_2PtCl_4 in water with downfield chemical shifts reported as positive. All of the chemical shifts and coupling constants are reported in parts per million and hertz, respectively. UV−vis spectra were recorded on a Varian Cary 50 spectrophotometer. Emission and excitation spectra were obtained by using a double monochromator Fluorolog 2 instrument from Spex. Fluorescence lifetimes were measured on a Timemaster model TM-3/2003 apparatus from PTI. The source was a nitrogen

laser equipped with a high-resolution dye laser (fwhm ~ 1500 ps), and the fluorescence lifetimes were obtained from deconvolution and distribution lifetime analysis.

Quantum Yield. The quantum yields were measured against [Ru(bpy)$_3$](Cl)$_2$ ($\Phi_e = 0.376 \pm 0.036$).[12]

X-Ray Crystallography. Single crystals of **11b** and **12** were coated with perfluoroalkyl ether oil (ABCR), mounted using a glass fiber, and frozen in the cold nitrogen stream of the goniometer. The data were collected on a Stoe IPDS diffractometer. The data were reduced (Integrate in IPDS) and corrected for absorption (FACEIT in IPDS). The structure was solved by direct methods and refined by full-matrix least-squares on F^2 (SHELXTL). Single crystals of **4b** were grown by slow vapor diffusion using methylethylketone as a good solvent and *tert*-butylmethylether at 298 K. One single crystal of 0.50 × 0.10 × 0.10 mm^3 was mounted using a glass fiber on the goniometer at 298(2) K. Data were collected on an Enraf-Nonius CAD-4 automatic diffractometer using ω scans. The DIFRAC[13] program was used for centering, indexing, and data collection. Two standard reflections were measured every 200 reflections; no intensity decay was observed during data collection. The data were corrected for absorption by empirical methods based on ψ scans and reduced with the NRCVAX[14] programs. All structures were solved using SHELXS-97[15] and refined by full-matrix least-squares on F^2 with SHELXL-97.[15] The non-hydrogen atoms were refined anisotropically. The hydrogen atoms were placed at idealized calculated geometric positions and refined isotropically using a riding model. The absolute structure of **4b** was determined by anomalous dispersion effect.[16] Crystallographic data have been deposited with the Cambridge Crystallographic Data Centre as CCDC 711384 (**4b**), CCDC 711703 (**11b**), and CCDC 711702 (**12**). Copies of the data can be obtained free of charge on application to Cambridge Crystallographic Data Centre, 12 Union Road, Cambridge CB2 1EZ, U.K. [fax: (+44) 1223−336−033; email: deposit@ccdc.cam.ac.uk).

Computational Details. Density functional theory (DFT) and time-dependent density functional theory (TDDFT) were performed with the commercial software Gaussian 03[17] using the Super Computer of the University of Sherbrooke (Mammouth MP) and supported by the Réseau Québécois de Calcul de Haute Performance. The TDDFT[18a−c] and DFT[18d−g] calculations were performed using the B3LYP method[19] with the basis sets 6-21g[20] for all C, N, and H atoms, whereas basis sets and specific core electron approximations were used for Pt, Pd, Cl, I, and P atoms.[21] The same basis sets were used to compute the electronic configuration of the triplet states and the energy of the highest semioccupied molecular orbitals (HSOMO) and the ground state (HOMO).[22]

Results and Discussion

1. The d^9−d^9 Homo- and Heterobimetallic Systems. The conclusion of our previous work on the reactivity of [ClM(μ-dppm)$_2$MCl] (M = Pd, Pt) toward isocyanides[10] urged us to synthesize additional derivatives ligated by one or two CNR ligands with diverging electronic and steric properties. A systematic variation of the nature of R in CNR ligands, of M, as well as of the halide ligands is necessary in order to elucidate what controls the bridging versus terminal coordination of the CNR ligands, as well as the photophysical properties of these compounds. This section describes the syntheses and characterization of some new isocyanide-containing homo- and heterobimetallic systems and discusses their structural features.

Grundy and Robertson previously demonstrated that treatment of [ClPt(μ-dppm)$_2$PtCl] (**2**) with *p*-tolylisocyanide in a CH_2Cl_2 solution affords the A-frame compound [ClPt(μ-dppm)$_2$(μ-C═N−C$_6$H$_4$Me)PtCl] (**4a**), resulting from CNR insertion on the Pt−Pt bond.[23] Surprisingly, treatment of **2** with xylylisocyanide (xylyl = 2,5-dimethylphenyl) in a 1:1 ratio under similar reaction conditions produces exclusively the Pt−Pt-bonded monocationic species [ClPt(μ-dppm)$_2$Pt(CNxylyl)]Cl (**3a**) bearing a terminal CNR ligand (Scheme 1). This terminal coordination mode can be inferred from the IR spectra, which exhibits a strong ν(C≡N) absorption at 2157 cm^{-1}. The ^{31}P{^{1}H} NMR spectra of **3a** give rise to AA′BB′ spin systems consisting of two multiplets centered at +1.2 and −1.7 ppm with $^1J_{Pt-P}$ couplings of 2370 and 3070 Hz, respectively. These observations contrast with a

(12) Demas, J. N.; Crosby, G. A. *J. Am. Chem. Soc.* **1971**, *93*, 2841–2847.
(13) Flack, H. D.; Blanc, E.; Schwarzenbach, D. *J. Appl. Crystallogr.* **1992**, *25*, 455–459.
(14) Gabe, E. J.; Le Page, Y.; Charland, J. P.; Lee, F. L.; White, P. S. *J. Appl. Crystallogr.* **1989**, *22*, 384–387.
(15) Sheldrick, G. M. *SHELXS 97*, Release 97-2; Sheldrick, G. M.; University of Göttingen: Göttingen, Germany, 1997.
(16) Flack, H. D. *Acta Crystallogr.* **1983**, *A39*, 876–881.
(17) Frisch, M. J.; Trucks, G. W.; Schlegel, H. B.; Scuseria, G. E.; Robb, M. A.; Cheeseman, J. R.; Montgomery, J. A., Jr.; Vreven, T.; Kudin, K. N.; Burant, J. C.; Millam, J. M.; Iyengar, S. S.; Tomasi, J.; Barone, V.; Mennucci, B.; Cossi, M.; Scalmani, G.; Rega, N.; Petersson, G. A.; Nakatsuji, H.; Hada, M.; Ehara, M.; Toyota, K.; Fukuda, R.; Hasegawa, J.; Ishida, M.; Nakajima, T.; Honda, Y.; Kitao, O.; Nakai, H.; Klene, M.; Li, X.; Knox, J. E.; Hratchian, H. P.; Cross, J. B.; Adamo, C.; Jaramillo, J.; Gomperts, R.; Stratmann, R. E.; Yazyev, O.; Austin, A. J.; Cammi, R.; Pomelli, C.; Ochterski, J. W.; Ayala, P. Y.; Morokuma, K.; Voth, G. A.; Salvador, P.; Dannenberg, J. J.; Zakrzewski, V. G.; Dapprich, S.; Daniels, A. D.; Strain, M. C.; Farkas, O.; Malick, D. K.; Rabuck, A. D.; Raghavachari, K.; Foresman, J. B.; Ortiz, J. V.; Cui, Q.; Baboul, A. G.; Clifford, S.; Cioslowski, J.; Stefanov, B. B.; Liu, G.; Liashenko, A.; Piskorz, P.; Komaromi, I.; Martin, R. L.; Fox, D. J.; Keith, T.; Al-Laham, M. A.; Peng, C. Y.; Nanayakkara, A.; Challacombe, M.; Gill, P. M. W.; Johnson, B.; Chen, W.; Wong, M. W.; Gonzalez, C.; Pople, J. A. *Gaussian 03*, revision C.2; Gaussian, Inc.: Wallingford, CT, 2004.
(18) (a) Stratmann, R. E.; Scuseria, G. E.; Frisch, M. J. *J. Chem. Phys.* **1998**, *109*, 8218–8224. (b) Bauernschmitt, R.; Ahlrichs, R. *Chem. Phys. Lett.* **1996**, *256*, 454–464. (c) Casida, M. E.; Jamorski, C.; Casida, K. C.; Salahub, D. R. *J. Chem. Phys.* **1998**, *108*, 4439–4449. (d) Hohenberg, P.; Kohn, W. *Phys. Rev.* **1964**, *136*, B864-B871. (e) Kohn, W.; Sham, L. J. *Phys. Rev.* **1965**, *140*, A1133-A1138. (f) Salahub; D. R.; Zerner, M. C. *The Challenge of d and f Electrons*; American Chemical Society: Washington DC, 1989. (g) Parr, R. G.; Yang, W. *Density-functional theory of atoms and molecules*; Oxford University Press: Oxford, U.K., 1989.
(19) (a) Becke, A. D. *J. Chem. Phys.* **1993**, *98*, 5648–5652. (b) Lee, C.; Yang, W.; Parr, R. G. *Phys. Rev. B: Condens. Matter Mater. Phys.* **1988**, 785–789. (c) Miehlich, B.; Savin, A.; Stoll, H.; Preuss, H. *Chem. Phys. Lett.* **1989**, *157*, 200–206.
(20) (a) Gordon, M. S.; Binkley, J. S.; Pople, J. A.; Pietro, W. J.; Hehre, W. J. *J. Am. Chem. Soc.* **1982**, *104*, 2797–2803. (b) Pietro, W. J.; Francl, M. M.; Hehre, W. J.; Defrees, D. J.; Pople, J. A.; Binkley, J. S. *J. Am. Chem. Soc.* **1982**, *104*, 5039–5048. (c) Dobbs, K. D.; Hehre, W. J. *J. Comput. Chem.* **1986**, *7*, 359–378. (d) Dobbs, K. D.; Hehre, W. J. *J. Comput. Chem.* **1987**, *8*, 861–879. (e) Dobbs, K. D.; Hehre, W. J. *J. Comput. Chem.* **1987**, *8*, 880–893.
(21) (a) Stevens, W. J.; Basch, H.; Krauss, M. *J. Chem. Phys.* **1984**, *81*, 6026–6033. (b) Stevens, W. J.; Krauss, M.; Basch, H.; Jasien, P. G. *Can. J. Chem.* **1992**, *70*, 612–630. (c) Cundari, T. R.; Stevens, W. J. *J. Chem. Phys.* **1993**, *98*, 5555–5565. (d) Binkley, J. S.; Pople, J. A.; Hehre, W. J. *J. Am. Chem. Soc.* **1980**, *102*, 939–947.
(22) Lowry, M. S.; Hudson, W. R.; Pascal, R. A., Jr.; Bernhard, S. *J. Am. Chem. Soc.* **2004**, *126*, 14129–14135.
(23) Grundy, K. R.; Robertson, K. N. *Organometallics* **1983**, *2*, 1736–1742.

Scheme 1

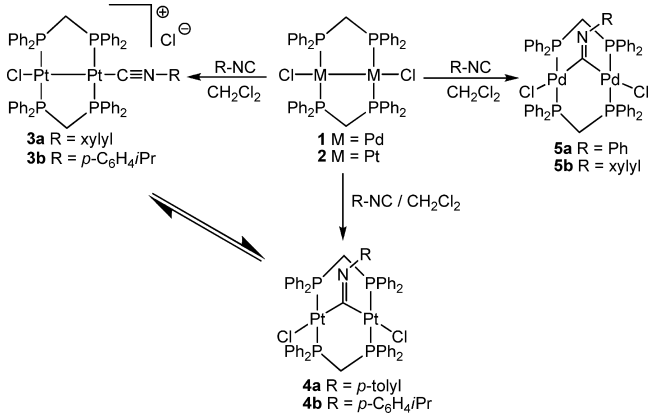

Scheme 2

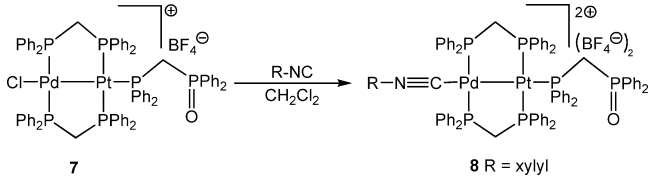

precedent report on the synthesis of [ClPd(μ-dppm)$_2$(μ-C═N−xylyl)PdCl] (**5b**) and [ClPd(μ-dppm)$_2$(μ-C═N−Ph)PdCl] (**5a**), spanned by a bridging CNR ligand.[24] These differences of behavior will be discussed later.

[ClPt(μ-dppm)$_2$Pt(CNxylyl)][BF$_4$]·CH$_2$Cl$_2$ (**3a′**) was prepared from the counterion metathesis of the Cl$^-$ salt (**3a**) with NaBF$_4$. Single crystals suitable for an X-ray structure analysis of this salt (**3a′**) were obtained, but because of the poor crystal quality, little data could be collected. Nevertheless, the collected data unambiguously demonstrated the conservation of the M−M bond (2.654 Å) and the terminal coordination of a linear RNC ligand (R−N(1)−C(49) = 175.4°; d(Pt(1)−C(49)) = 1.93 Å) at Pt(1) (Figure S2, Supporting Information). These values compare favorably to those recently reported for the dicationic salt [(iPrC$_6$H$_4$NC)Pt(μ-dppm)$_2$Pt(CNC$_6$H$_4$$i$Pr)](BF$_4$)$_2$, having a Pt−Pt bond length of 2.6453(3) Å and two linearly bonded CNR ligands with mean Pt−C bond distances of 1.99 Å.[5]

The cationic heterodinuclear complex [ClPd(μ-dppm)$_2$Pt(η^1-dppm═O)](BF$_4$) (**7**), coordinated by a dangling diphosphine oxide, reacts with a stoichiometric amount of xylylisocyanide to produce the dicationic salt [(xylylNC)Pd(μ-dppm)$_2$Pt(η^1-dppm═O)](BF$_4$)$_2$ (**8**) after a metathesis reaction exchanging the counterion Cl for BF$_4$. (Scheme 2). The RNC terminal coordination on Pd is readily deduced from the IR spectrum, which exhibits a strong ν(C≡N) absorption at 2167 cm^{-1}. The ^{31}P{^{1}H} NMR spectrum of **8**, which is similar to that of precursor **7**, is reported in the Supporting Information.

An interesting borderline case between RNC terminal ligation in M−M connected d^9−d^9 systems and μ-CNR coordination giving rise to d^8−d^8 A-frame bimetallics is compound **10a** (Scheme 3), which exists in two isomeric

Scheme 3

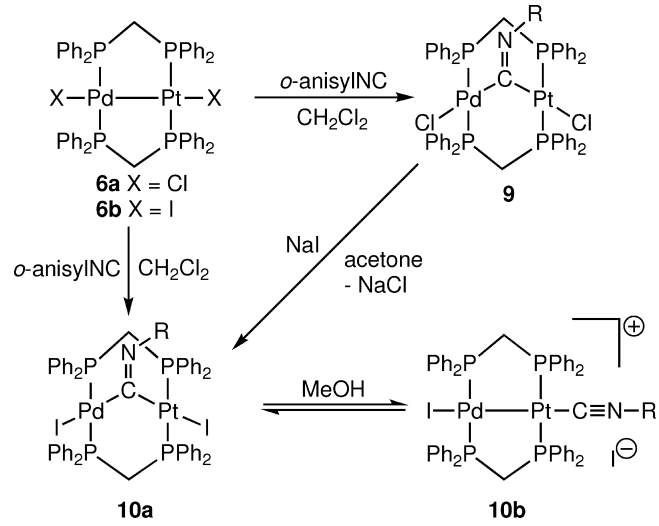

forms. This dinuclear iodo complex is obtained by the treatment of [IPd(μ-dppm)$_2$PtI] (**6b**) with 1 equiv of o-anisylisocyanide in CH$_2$Cl$_2$ or by halide metathesis with NaI using [ClPd(μ-dppm)$_2$(μ-C═N-o-anisyl)PtCl] (**9**) as a precursor. This yellow compound prevails in the crystalline state almost exclusively in the A-frame form [IPd(μ-dppm)$_2$(μ-C═N-o-anisyl)PtI] (**10a**), as deduced from the observed IR-active ν(C═N) at 1611 cm^{-1}. However, the IR spectrum of **10a** in CH$_2$Cl$_2$ solution indicates the coexistence of an appreciable percentage of the ionic form [IPd(μ-dppm)$_2$Pt(CN-o-anisyl)]I (**10b**) with a terminal coordinated CNR ligand. This equilibrium is entirely shifted in a 1:1 MeOH/CH$_2$Cl$_2$ mixture toward the ionic isomer **10b**. Owing to the increase in solvent polarity, the dissociation of the iodo ligand is now facilitated. Indeed, a single sharp ν(C≡N) band is detected at 2175 cm^{-1} in the IR spectrum of **10b**.

The equilibrium in solution can also be monitored by ^{31}P{^{1}H} NMR spectroscopy. The spectra exhibit an approximate 50:50 distribution between **10a** and **10b** in a 1:1 CDCl$_3$/CH$_2$Cl$_2$ mixture. However, in 1:1 CDCl$_3$/MeOH as a solvent medium, only a small amount of the A-frame isomer **10a** remains detectable (Figure 1). The AA′BB′-type resonances of **10b** appear at strongly high-field regions at −3.1 (P_{Pt}) and −8.9 ppm (P_{Pd}) in comparison with those of the μ-CNR isomer **10a** (AA′BB′ type, 10.8 (P(Pt)) and 12.3 ppm (P_{Pd})). The Pt−Pd bond scission also causes a considerable increase of the $^1J_{Pt-P}$ couplings going from 2590 to 3465 Hz. The ^{195}Pt{^{1}H} NMR spectrum of **10b** consists of a broadened triplet of triplets centered at −2758 ppm with $^1J_{Pt-P}$ and $^{2+3}J_{Pt-P}$ couplings of 2590 and 50 Hz, respectively.

The observation of isomers' equilibrium, even in a less polar medium such as CDCl$_3$/CH$_2$Cl$_2$, suggests that the energetic difference between bridging and terminal RNC bonding is quite small in system **10**. The solvent polarity dependence on the CNR coordination mode was already noticed by others.[25] Examples include the p-tolyl isocyanide adduct of [ClPt(μ-

(24) (a) Khan, M. A.; McAlees, A. J. *Inorg. Chim. Acta* **1985**, *104*, 109–114. (b) Benner, L. S.; Balch, A. L. *J. Am. Chem. Soc.* **1978**, *100*, 6099–6106.

(25) (a) Uson, R.; Fornies, J.; Espinet, P.; Fortuno, C. *J. Chem. Soc., Dalton Trans.* **1986**, 1849–1855. (b) Fornies, J.; Martinez, F.; Navarro, R.; Redondo, A.; Tomas, M.; Welch, A. J. *J. Organomet. Chem.* **1986**, *316*, 351–366.

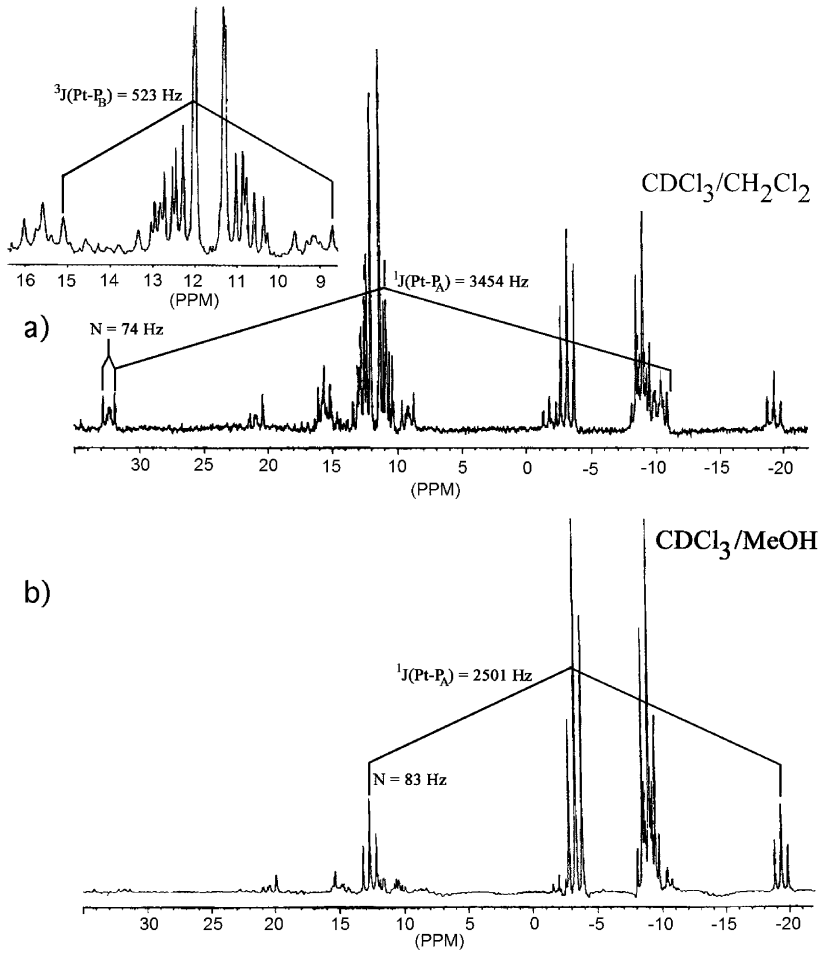

Figure 1. (a) ^{31}P{^{1}H} NMR spectrum of an isomeric mixture of **10a** and **10b** recorded in $CDCl_3/CH_2Cl_2$. (b) ^{31}P{^{1}H} NMR spectrum of **10b** recorded in $CDCl_3/CH_3OH$ ($N = |^2J(P_AP_B) + {}^4J(P_AP_{B'})|$).

dppm)$_2$PtC$_6$F$_5$], which exists in benzene as the A-frame [ClPt(μ-dppm)$_2$(μ-C═N-*p*-tolyl)PtC$_6$F$_5$] but rearranges entirely in CH_2Cl_2 to the ionic [(*p*-tolyl-N≡C)Pt(μ-dppm)$_2$PtC$_6$F$_5$]Cl form. The low, but definite, conductivity of the heterodinuclear [ClPt(μ-dppm)$_2$(μ-C═N-*p*-tolyl)PdC$_6$F$_5$] complex-containing acetone solution was ascribed to a deinsertion−terminal coordination equilibrium. All in all, system **10** represents the first case where a coexistence of d^8−d^8 and d^9−d^9 isomers of the Ni-triad in a noncoordinating solvent is established.

2. The d^8−d^8 A-Frame Homo- and Heterobimetallic Systems. In contrast with the stoichiometric reaction of **2** with xylylisocyanide affording the cationic complex [ClPt(μ-dppm)$_2$Pt(CNxylyl)]Cl (**3a**), the treatment of **2** with 1-isocyano-4-isopropylbenzene in CH_2Cl_2 yields, as previously, a mixture of the A-frame compound [ClPt(μ-dppm)$_2$(μ-C═N−C$_6$H$_4$*i*Pr)PtCl] (**4b**) and the ionic compound [ClPt(μ-dppm)$_2$Pt(CNC$_6$H$_4$*i*Pr)]Cl (**3b**) (Scheme 4; see Table 1 for Crystal and Refinement Data).

The existence of these two isomeric forms can be deduced from the IR (in CH_2Cl_2, ν(C═N) = 1616; ν(N≡C) = 2162 cm^{-1}) and the ^{31}P{^{1}H} NMR spectra. The spectra exhibit an approximate 50:50 distribution between **4b** and **3b** in $CDCl_3$ at 298 K. The AA′BB′-type resonances of **3b** appear at 3.4 and 7.5 ppm, whereas the resonance of μ-CNR isomer **4b** is

Scheme 4

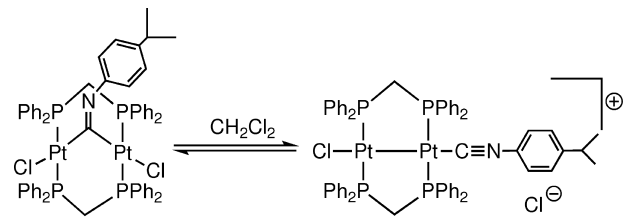

4b **3b**

a singlet at 17.5 ppm. The shift and the types of resonances obtained for **3b** compare unambiguously with the data reported above for [ClPt(μ-dppm)$_2$Pt(CNxylyl)]BF$_4$ (**3a′**).

Crystal Structure of 4b. In contrast with several reports on the molecular structures of μ-CNR-containing d^8−d^8 Pd$_2$ A-frame systems, no crystallographic information on analogous Pt$_2$ compounds was available until this work. The insertion of CN−C$_6$H$_4$*i*Pr into the Pt−Pt bond was corroborated by the X-ray diffraction study (Figure 2, Table 2). The overall structure of **4b** resembles that of the corresponding Pd$_2$ A-frame complex [ClPd(μ-dppm)$_2$(μ-C═N−Ph)PdCl].[24a,26]

Similarly to the previous complex (d(Pd···Pd) = 3.188(1) Å),[24a] the insertion causes a considerable elongation of M···M interactions (d(Pt···Pt) 3.2118(18) Å), and the *C*═N-R angle is somewhat less acute (133.0(2) vs 129.3(9)°). The coordination modes about the Pt atoms are square-planar

Table 1. Crystal and Refinement Data for **4b**, **11b**, and **12**

	4b	**11b**·0.5CH_2Cl_2	**12**·CH_2Cl_2
empirical formula	$C_{60}H_{55}Cl_2NP_4Pt_2$	$C_{66.5}H_{59}ClI_2N_2O_2P_4PdPt$	$C_{64}H_{62}Cl_2I_2OP_4PdPt$
fw	1375.01	1632.78	1625.23
description	colorless	orange	orange
cryst size (mm)	0.10 × 0.10 × 0.5	0.20 × 0.20 × 0.10	0.30 × 0.20 × 0.20
temp (K)	293(2)	173(2)	173(2)
cryst syst	tetragonal	orthorhombic	monoclinic
space group	*P*41	*Pbca*	*P*2(1)/*c*
a (Å)	21.510(4)	15.658(2)	21.703(4))
b (Å)	21.510(4)	24.377(4)	13.373(3)
c (Å)	14.2270(13)	32.281(5)	24.493(5)
β (^{deg})	90	90	115.04(3)
Vol (Å^3)	6583(2)	12321(3)	6441(2)
Z	4	8	4
calcd. density (Mg/m^3)	1.387	1.760	1.676
scan mode	ω	φ	φ
F(000)	2688	6360	3168
abs coeff (mm^{-1})	9.747	3.756	3.631
θ range	4.11−69.98°	1.26−25.00°	2.24−25.00°
limiting indices	$0 \le h \le 26$	$-18 \le h \le 26$	$-24 \le h \le 25$
	$-26 \le k \le 0$	$-28 \le k \le 28$	$-15 \le k \le 15$
	$-17 \le l \le 0$	$-38 \le l \le 38$	$-29 \le l \le 29$
reflns collected	6385	229876	41644
independent reflns	6385	10851	11321
min./max.transmiss. ratio	0.4423/0.0848	0.7052/0.5205	0.5304/0.4089
data /restraints/ params	3556/371/478	10851/2/727	11321/0/693
goodness-of-fit on F^2	1.034	1.081	1.012
final R indices $[I > 2\sigma(I)]^a$	R1 = 0.0880	R1 = 0.0620	R1 = 0.0848
	wR2 = 0.2308	wR2 = 0.1466	wR2 = 0.2447
R indices (all data)	R1 = 0.1524	R1 = 0.0842	R1 = 0.0990
	wR2 = 0.2884	wR2 = 0.1550	wR2 = 0.2561

^{a} $R1 = \sum||F_o| - |F_c||/\sum |F_o|$; $wR2 = (\sum[w(F_o^2 - F_c^2)^2]/\sum[F_o^4])^{1/2}$; weight $= 1/[\sigma^2(F_o^2) + (A\cdot P)^2 + (B\cdot P)]$ where $P = (\max(F_o^2,0) + 2F_o^2)/3$, $A = 0.0890$ and $B = 11.4580$ for **4b**, $A = 0.0612$ and $B = 161.0473$ for **11b**, and $A = 0.1686$ and $B = 50.39$ for **12**.

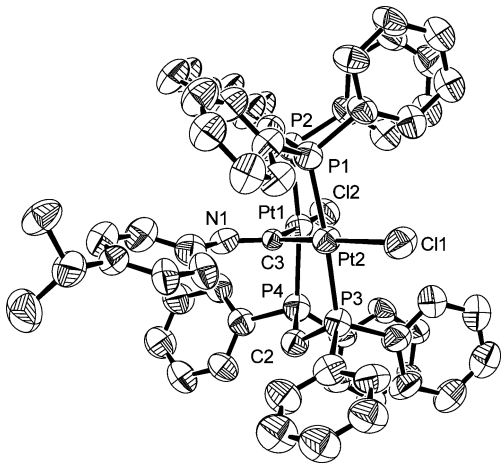

Figure 2. Thermal ellipsoid plot of **4b** at the 30% probability level. The H atoms are omitted for clarity. A colored ball-and-stick representation of **4b** with the numbering scheme is available in the Supporting Information.

Table 2. Selected Bond Distances (Å) and Angles (deg) for **4b**

Pt(1)−C(3)	1.92(2)	Pt(1)−P(2)	2.290(9)
Pt(2)−C(3)	1.97(2)	Pt(1)−P(4)	2.292(9)
C(3)−N(1)	1.31(3)	Pt(2)−P(1)	2.289(8)
Pt(1)−Cl(2)	2.443(10)	Pt(2)−P(3)	2.279(9)
Pt(2)−Cl(1)	2.446(8)	C(4)−N(1)	1.41(3)
Pt···Pt	3.2118(18)		
Cl(2)−Pt(1)−C(3)	175.8(7)	P(1)−Pt(2)−C(3)	88.1(6)
Cl(1)−Pt(2)−C(3)	176.8(7)	P(3)−Pt(2)−C(3)	86.9(6)
P(4)−Pt(1)−C(3)	84.7(7)	P(2)−Pt(1)−C(3)	87.6(7)
P(4)−Pt(1)−P(2)	171.0(4)	P(2)−Pt(1)−Cl(2)	93.03(3)
P(3)−Pt(2)−P(1)	175.0(3)	P(4)−Pt(1)−Cl(2)	94.3(3)
Pt(1)−C(3)−Pt(2)	110.9(11)	P(3)−Pt(2)−Cl(1)	91.1(3)
P(1)−Pt(2)−Cl(1)	93.9(3)	C(3)−N(1)−C(4)	133.0(2)
P(2)−C(1)−P(1)	115.9(15)	P(3)−C(2)−P(4)	114.6(17)

and share bridging C(3), which spans in a symmetric manner the two Pt centers. The Pt−C(3) bond lengths of 1.92(2) and 1.97(2) Å resemble the Pd−μ-C distances in the Pd_2 complex (1.99(1) and 1.96(1) Å). The Pt(1)−C(3)−Pt(2) angle of 110.9(11)° is also close to the reported Pd(1)−C(3)−Pd(2) angle of 107.5(5)° for [ClPd(μ-dppm)$_2$(μ-C═N−Ph)-PdCl].[24a]

The question now arises as to why the addition of *p*-tolylisocyanide in a CH_2Cl_2 solution produces the A-frame compounds **4a**, whereas under analogous reaction conditions, the treatment of **2** with xylylisocyanide leads to the d^9-d^9 salt **3a′**. Steric effects are unlikely despite the bulkiness of the xylyl group, since in the case of the d^8-d^8 Pd···Pd system **5b**, the xylylNC ligand adopts, without any steric repulsion, a bridging position.

Hypothetically, electronic effects of the aryl substituent R are likely responsible for the bonding mode of the ArNC ligand. Theoretical studies on substituent effects on the frontier MOs of *o*- and *p*-substituted ArNC illustrated that (*i*) the substitution position (ortho vs para) does not appreciably alter the electron density of the donor group; (*ii*) phenyl ring substitution has a *smaller* effect on the σ-donating ability than it does on the π-accepting propensity of the ArNC ligand; and (*iii*) the π-accepting abilities of the isocyanide ligands increase in the order *o*-, *p*-$CH_3OC_6H_4NC$; *o*-, *p*-$CH_3C_6H_4NC$; *o*-, *p*-C_6H_5NC; *o*-, *p*-FC_6H_4NC; *o*-, *p*-$CF_3C_6H_4NC$; *o*-, *p*-ClC_6H_4NC; and *o*-, *p*-$NO_2C_6H_4NC$, while the σ-donating ability decreases in this same order.[27]

The *p*-tolyl and xylylisocyanide ligands both exhibit methyl substituents. On the basis of the above theoretical findings, the

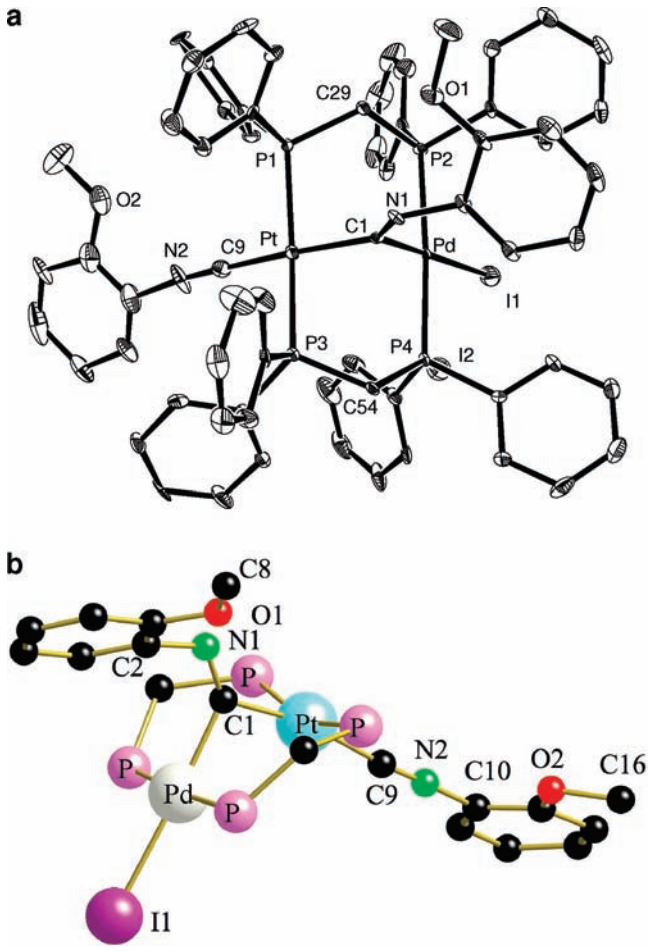

Figure 3. (a) Thermal ellipsoid plot of **11b** at the 30% probability level. The H atoms are omitted for clarity. A colored ball-and-stick representation with a numbering scheme is available in the Supporting Information. (b) View of the core structure of **11b**.

Table 3. Selected Bond Distances (Å) and Angles (deg) for **11b**

Pt−C(1)	2.014(10)	Pt−P(3)	2.323(3)
Pd−C(1)	2.013(10)	Pd−P(4)	2.340(3)
C(1)−N(1)	1.264(12)	Pd−P(2)	2.336(2)
Pd−I(1)	2.7213(11)	Pt−P(1)	2.323(3)
Pt−C(9)	1.987(12)	C(9)−N(2)	1.123(14)
Pt···Pd	3.0273(9)	C(10)−N(2)	1.462(16)
C(9)−Pt−C(1)	168.6(4)	P(1)−Pt−C(1)	83.9(3)
I(1)−Pd−C(1)	177.3(3)	P(3)−Pt−C(1)	88.8(3)
P(1)−Pt−C(9)	97.6(3)	P(1)−Pt−C(9)	97.6(3)
P(1)−Pt−P(3)	158.87(9)	P(2)−Pd−I(1)	95.61(7)
P(2)−Pd−P(4)	175.57(9)	P(4)−Pd−I(2)	93.74(8)
Pd−C(1)−Pt	97.5(4)	Pt−C(9)−N(2)	175.2(10)
C(1)−N(1)−C(2)	122.8(8)	C(9)−N(2)−C(10)174.3(15)	
P(2)−C(29)−P(1)	117.4(5)	P(3)−C(54)−P(4)	115.7(5)

relevant MO energies are affected little by the *o*- or *p*-substitution with respect to the nature of the substituent. Therefore, the *subtle* additional electron-donating effect of the second methyl group of xylylisocyanide may cause a switching of the CNR bonding mode from bridging to terminal (**4a** vs **3a**). In **4b**, the isopropyl substituent at the *p*-position likely exerts a slightly stronger electron-donating induction effect than methyl does, but in overall σ-donor/π-acceptor propensity, xylylisocyanide seems to be a somewhat better donor ligand than 1-isocyano-4-isopropylbenzene. In addition, one notes the strong bending of the μ-C═N−R angle (123−135°) observed for all homo- and heterodinuclear A-frame complexes. Although

Scheme 5

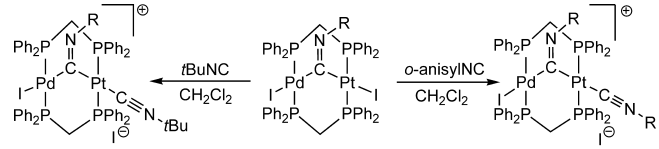

12 R = *o*-anisyl **10a** **11b** R = *o*-anisyl

bridging is often associated with bending of the μ-C═N−R angle, this structural feature is not so obvious. There are several examples in the literature for di- and polynuclear clusters exhibiting linear μ_2-CNR ligands. One example is [(py)ClPd(μ-CN−xylyl)$_2$PdCl(py)], spanned by two isocyanides with C−N−C angles of 175.2(13) and 157.9(9)°.[28a] The steric factors are not important in determining the C−N−C angles since the more linear ligand is associated with the less hindered position on the dinuclear Pd_2 complex. An electronic origin was also suggested to explain the observed μ-CNR linearity (171.4(8) and 168.4(7)°) in [$Pd_5(\mu\text{-}SO_2)_3(\mu\text{-}C{=}N{-}xylyl)_2(CNxylyl)_5$].[28b] Howell et al. computed the MeNC bonding properties and predicted that, regardless of the molecular geometry, the CNR σ-donor character remains essentially constant, but the π-acceptor capacity strongly depends on the C═N−R angle and may even reach that of carbon monoxide, if the degree of bending is significant enough.[29]

All A-frame complexes of the type [LM(μ-dppm)$_2$(μ-C═N−R)ML] contain four electron-donating bidentate phosphorus ligands. This donation in these electron-rich systems could be, at least, partially compensated by back-bonding in the μ-CNR ligand π^* orbitals (push−pull). On the basis of calculations,[29] the C═N−R angle must be < 140° to consider the isocyanide ligand as a good π-acceptor. This may explain the marked bending observed in **4b**, **11b**, and **14** (see X-ray structures below). Packing effects may also influence the degree of bending in the solid state.

The heterodinuclear complex [ClPd(μ-dppm)$_2$(μ-C═N-*o*-anisyl)PtCl] (**9**) results from the insertion of 1 equiv of *o*-anisylisocyanide into the Pd−Pt bond of [ClPd(μ-dppm)$_2$PtCl] (**6a**). In contrast to its iodo analogue **10**, compound **9** exists in CH_2Cl_2 solution solely in the A-frame form. This finding demonstrates that, apart from the solvent polarity, the nature of the halide ligand also plays an important role in the subtle balance between bridging and terminal isocyanide bonding.

The iodo derivative **10a** can also be used as precursor for the synthesis of bis(isonitrile) heterobimetallics, allowing the study of site selectivity in the second CNR ligand coordination, Pd versus Pt. Hence, upon the addition of 1 equiv of *o*-anisylisocyanide, exclusive formation of [IPd(μ-dppm)$_2$(μ-C═N-*o*-anisyl)Pt(CN-*o*-anisyl)]I (**11b**; Figure 3, Table 3), exhibiting both a μ-CNR and a Pt-bound terminal CNR ligand, is observed (Scheme 5). This air-stable orange-red salt was unambiguously identified by IR and multinuclear NMR spectroscopy as well as by a single-crystal X-ray diffraction study.

The terminal ν(C≡N) and bridging ν(C═N) absorptions of **11b** in CH_2Cl_2 are observed at 2175 and 1627 cm^{-1}, respectively. In comparison with precursor **10**, the $^{31}P\{^1H\}$ NMR signals resonate downfield at 15.0 (P_{Pt}) and 20.8 (P_{Pd})

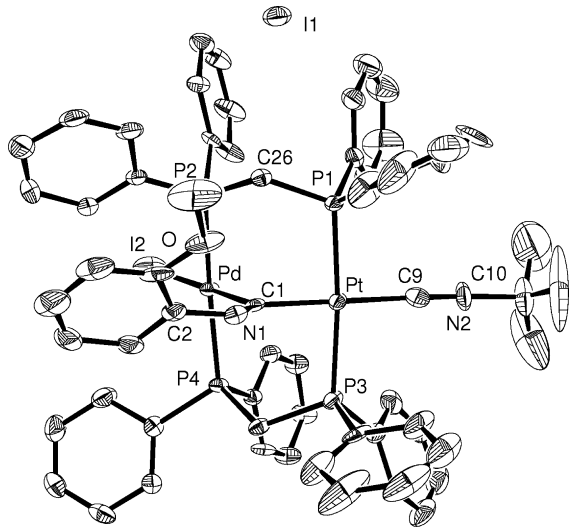

Figure 4. Thermal ellipsoid plot of **12** at the 30% probability level. The H atoms are omitted for clarity. A colored ball-and-stick representation of **12** with a numbering scheme is available in the Supporting Information.

Table 4. Selected Bond Distances (Å) and Angles (deg) for **12**

Pt−C(1)	2.010(13)	Pt−P(3)	2.298(3)
Pd−C(1)	2.018(10)	Pd−P(4)	2.366(3)
C(1)−N(1)	1.277(17)	Pd−P(2)	2.337(3)
Pd−I(1)	2.7116(18)	Pt−P(1)	2.321(3)
Pt−C(9)	1.98(2)	C(9)−N(2)	1.16(2)
Pt···Pd	3.2085(12)	C(10)−N(2)	1.511(19)
C(9)−Pt−C(1)	179.6(6)	P(1)−Pt−C(1)	86.3(3)
I(1)−Pd−C(1)	178.4(4)	P(3)−Pt−C(1)	85.4(3)
P(1)−Pt−C(9)	93.3(4)	P(3)−Pt−C(9)	95.0(4)
P(1)−Pt−P(3)	158.87(9)	P(4)−Pd−I(1)	88.48(7)
P(2)−Pd−P(4)	175.57(9)	P(2)−Pd−I(1)	95.61(7)
Pd−C(1)−Pt	97.5(4)	Pt−C(9)−N(2)	178.0(18)
C(1)−N(1)−C(2)	124.0(11)	C(9)−N(2)−C(10)1	76.0(2)
P(2)−C(26)−P(1)	114.9(6)	P(3)−C(51)−P(4)	115.0(6)

ppm. The ^{195}Pt{^{1}H} NMR of **11b** contains a well-resolved triplet of triplet resonance centered at −2825 ppm with $^1J_{Pt-P}$ and $^3J_{Pt-P}$ couplings of 3225 and 300 Hz, respectively. Despite the nonequivalence of the OCH_3 groups, a single sharp resonance is found at 55.9 ppm in the ^{13}C{^{1}H} NMR spectrum (298 K). This fast CNR ligand exchange on the NMR time scale is also concluded from the single resonance observed at 3.45 ppm in the ^{1}H NMR spectrum at 273 K, whereas the CH_2−dppm (3.28 ppm) and the aromatic hydrogens are quite large without any fine structure. Coalescence occurs at about 243 K, since a broad hump including the CH_2−dppm and OCH_3 groups is observed in the 3.65−3.15 ppm region. At 233 K, two new broad singlets emerge at 3.60 and 3.21 ppm, which are attributed to two distinct OCH_3 groups. Progressive cooling to 213 K causes a sharpening and splitting of the two OCH_3 signals (3.63 and 3.17), whereas the CH_2−dppm protons appear in the form of an unstructured broad signal at 3.46 ppm.

The Cl-analogue [ClPd(μ-dppm)$_2$(μ-C═N-*o*-anisyl)Pt(C≡N-*o*-anisyl)]Cl (**11a**) was also prepared (^{195}Pt{^{1}H}: triplet of triplets at −2856 ppm with $^1J_{Pt-P}$ and $^3J_{Pt-P}$ of 3210 and 302 Hz, respectively). Variable-temperature ^{1}H NMR monitoring also showed a similar fluxional behavior, albeit at higher temperatures (the fast exchange occurs at 313 K). The exchange phenomenon of the isocyanide coordinations was also previously noticed by Balch and Benner[24] and Kubiak and Kullberg[30] for [(R−N≡C)]Pd(μ-"R_2PCH_2PR"$_2$)$_2$(μ-C═N−R)Pd(C≡N−R)]$^{2+}$ (R′ = Me, Ph). Puddephatt and collaborators also reported intramolecular terminal-bridge isocyanide exchanges in $Pt_3(dppm)_3^{2+}$-type clusters, processes believed to be due to small energy barriers.[31]

The salt [IPd(μ-dppm)$_2$(μ-C═N-*o*-anisyl)Pt(C≡N*t*Bu]I (**12**) can also be isolated as an air-stable orange solid after the addition of 1 equiv of *t*BuNC to **10** (Figure 4, Table 4). As unambiguously confirmed by an X-ray diffraction study, the additional terminal CNR is again coordinated at the Pt site. The *o*-anisyl isocyanide occupies the bridging position, since it is a better π acceptor compared to *t*BuNC. Indeed, it can compensate more efficiently the electron donation exerted by the two dppm ligands.[32] To our knowledge, **12** is the first example of an A-frame system of the Ni-triad bearing two different isocyanide ligands. As expected, the pattern and couplings of the AA′BB′ ^{31}P{^{1}H} and ^{195}Pt{^{1}H} NMR spectra resemble those of **11b**. The ^{195}Pt signal is somewhat high-field-shifted to −2860 ppm with $^1J_{Pt-P}$ and $^3J_{Pt-P}$ couplings of 3220 and 325 Hz, respectively. In the ^{1}H NMR spectrum at 295 K, the OCH_3 and *tert*-butyl groups give rise to sharp singlets at 3.43 and 0.86 ppm; however, the CH_2−dppm centered at 3.16 ppm is unresolved. The question arises why the displacement reaction of X^- by a second CNR ligand takes place at platinum rather than palladium. Substitution reactions at Pd are known to be much faster than at Pt, but the positive charge of the resulting cationic salts **11** and **12** is probably better stabilized on the more electron-rich Pt(I) center. Furthermore, generation of a new Pt−C bond instead of a Pd−C bond may also be more favorable for thermodynamic reasons.

Crystal Structures of 11b and 12. The X-ray structure of **11b** confirms the proposed A-frame structure of the complex in solution at low temperatures (deduced from NMR measurements). The coordination sphere about palladium and platinum is nearly planar with the two squares connected at one corner by the bridging CNR. The other coordination sites in trans disposition relative to the μ-C atom are occupied by a second CNR ligand and an I atom on the Pt and Pd metals, respectively. The extreme inclination of the μ-C═N-*o*-anisyl

(26) (a) Hanson, A. W.; McAlees, A. J.; Taylor, A. *J. Chem. Soc., Perkin Trans. 1* **1985**, 441–446. (b) Olmstead, M. M.; Hope, H.; Benner, L. S.; Balch, A. L. *J. Am. Chem. Soc.* **1977**, *99*, 5502–5503.
(27) (a) Johnston, R. F.; Cooper, J. C. *THEOCHEM* **1991**, *236*, 297–307. (b) Csonka, I. P.; Szepes, L.; Modelli, A. *J. Mass. Spectrom.* **2004**, *39*, 1456–1466.
(28) (a) Yamamoto, Y.; Yamazaki, H. *Inorg. Chem.* **1986**, *25*, 3327–3329. (b) Burrows, A. D.; Fleischer, H.; Mingos, D. M. P. *J. Organomet. Chem.* **1992**, *433*, 311–321.
(29) Howell, J. A. S.; Saillard, J. Y.; Le Beuze, A.; Jaouen, G. *J. Chem. Soc., Dalton Trans.* **1982**, 2533−2537.
(30) Kullberg, M. L.; Kubiak, C. P. *Inorg. Chem.* **1986**, *25*, 26–30.
(31) Bradford, A. M.; Kristof, E.; Rashidi, M.; Yang, D.-S.; Payne, N. C.; Puddephatt, R. J. *Inorg. Chem.* **1994**, *33*, 2355–2363.
(32) (a) Knorr, M.; Braunstein, P.; Strohmann, C. *Organometallics* **1996**, *15*, 5653–5663. (b) Knorr, M.; Strohmann, C. *Eur. J. Inorg. Chem.* **1998**, *49*, 5–499. (c) Knorr, M.; Strohmann, C. *Organometallics* **1999**, *18*, 248–257. (d) Knorr, M.; Strohmann, C. *Eur. J. Inorg. Chem.* **2000**, *24*, 1–252. (e) Knorr, M.; Jourdain, I.; Lentz, D.; Willemsen, S.; Strohmann, C. *J. Organomet. Chem.* **2003**, *684*, 216–229. (f) Knorr, M. *Reactivity and activation of small molecules on heterobimetallic complexes*, Habilitation thesis, University of the Saarland, Saarbrücken, Germany, 1996.

Chart 2

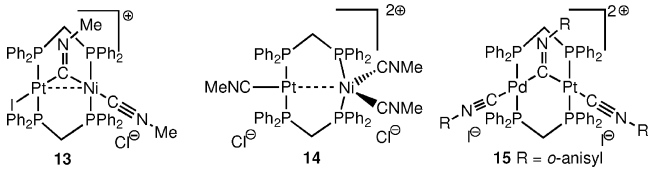

Chart 3

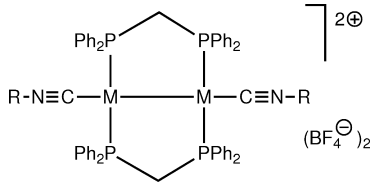

16 (M = Pd; R = 2,5-$Me_2C_6H_3$)
17 (M = Pt; R = 4-C_6H_4-*i*Pr)

ligand of 122.8(8)° is much more pronounced than that of **4b**, whereas the terminal CN-*o*-anisyl ligand is quite linear with an angle C(9)−N(2)−C(10) of 174.1(15)°. Consistent with a formal C═N double-bond character, the C(1)−N(1) distance is markedly longer than the C(9)−N(2) triple bond (1.264(12) vs 1.123(14) Å).

The terminal coordination of *t*BuNC at Pt is confirmed by the structure determination of **12**. In comparison with **11b**, the M···M′ separation has increased from 3.0273(9) to 3.2085(12) Å. As in **11b**, the μ-C═N−R ligand is strongly bent ((124.0(11)°), the anisyl ring being tilted toward the PdP_2I moiety. Again, the spanning of the two M centers is almost symmetric with Pt−C(1) and Pd−C(1) bond distances of 2.010(13) and 2.018(10) Å, respectively. The bond length between Pt and the terminal *t*BuNC ligand (Pt−C(9) 1.98(2) Å) is identical to that of [(OC)$_3$Fe{Si(OMe)$_3$}(μ-dppm)Pt(CN-*t*Bu){C(C═O)Me}] (1.989(8) Å).[32a] As in **4b**, the CH_2−dppm groups of **11b** and **12** are bent toward the μ-CNR ligand, leading to a "boat" conformation of the $M_2P_4C_2$ rings.

Complexes **11** and **12** are rare examples of heterobimetallic MM′ complexes spanned by a μ-CNR ligand. The other example is [ClPt(μ-dppm)$_2$(μ-C═N−Me)Ni(CNMe)]Cl (**13**) reported by Kubiak et al. via a transmetalation of [(CN-Me)]Ni(μ-dppm)$_2$(μ-C═N−Me)Ni(CNMe)] with [Cl_2Pt-(dppm)].[33] Like in **11** and **12**, the μ-CNR ligand is strongly bent (132.3°), and the MeNC ligands are equivalent in solution on the ^{1}H NMR time scale, indicating fluxionality.

There are however some striking differences between the Ni−Pt and Pd−Pt systems: (i) in **13** (Chart 2), the two M centers are connected through a short Ni−Pt bond of 2.5892(9) Å, (ii) the terminal MeNC ligand is bonded to the Ni center, whereas the halide ligand is coordinated on Pt, and (iii) halide abstraction in the presence of 1 equiv of MeNC produces the tris(isocyanide) compound **14** exhibiting a penta-coordinated Ni center. In contrast, the addition of an excess of *o*-anisylNC to **11b** leads to the formation of the A-frame dication **15**. In comparison with **10** and **11b**, the ^{31}P{^{1}H} NMR signals also appear more downfield at 19.0 (P_{Pt}) and 24.8 ppm (P_{Pd}) with $^1J_{Pt-P}$ and $^3J_{Pt-P}$ couplings of

(33) Ratliff, K. S.; Fanwick, P. E.; Kubiak, C. P. *Polyhedron* **1990**, *9*, 2651–2653.

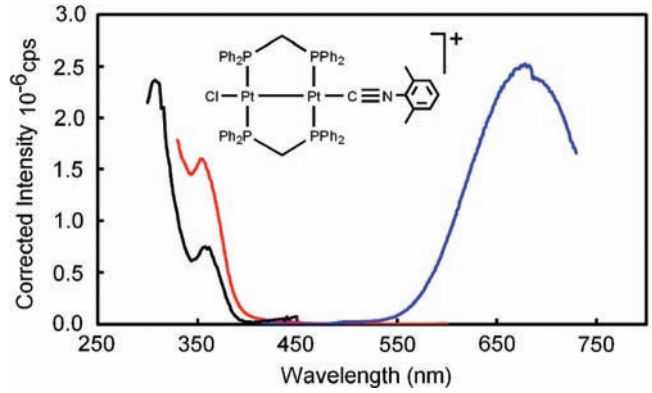

Figure 5. Absorption (black), excitation (red), and emission (blue) spectra of **3a′** in PrCN at 77 K. λ_{exc} = 370 nm.

3096 and 390 Hz, respectively. The ^{195}Pt{^{1}H} NMR spectrum exhibits quite a broad triplet-of-triplet resonance centered at −2924 ppm. Complex **15** could not be isolated purely, as mainly **11b** was recovered after recrystallization. The facile dissociation of the third CNR ligand was also noticed earlier for [(RNC)Pt(μ-dppm)$_2$(μ-C═N−R)Pt(CNR)]$^{2+}$ and [(RNC)Pd-(μ-dppm)$_2$(μ-C═N−R)Pd(CNR)]$^{2+}$ (R = Me, xylyl).[23,30,34]

3. Electronic Spectra and Photophysics. 3.1. Photophysical Properties of the d^9−d^9 Homo- and Heterobimetallic Systems. Many CNR-containing d^9−d^9 compounds, such as **16** and **17** (Chart 3), exhibit luminescence at room temperature in the solid state and at 77 K in frozen solution,[5] while the binuclear complexes **1**, **2**, and **6a** do not. Generally, Pd-containing materials exhibit much less luminescence intensity than the Pt-containing analogues. In addition, the replacement of the two axial chloride ligands in **1** and **2** by acetonitrile leads to the corresponding [(MeCN)M(μ-dppm)$_2$M(NCMe)]$^{2+}$ complexes (M = Pd, Pt), which are also weakly emitting.[5] This brings the question, what does it take to render these d^9−d^9 Pd_2- and Pt_2(dppm)$_2$-containing building blocks luminescent. Part of the answer lies in the presence of luminescence of bisphosphine and bis(pyridine-like)-containing d^9−d^9 "Pt(μ-dppm)Pt" complexes in solution at room temperature.[35]

Dissymmetric compound **3a′**, which contains one axially substituted position by a xylyl−NC ligand, exhibits a weak luminescence at 77 K (Figure 5). The excitation spectrum superposes the absorption unambiguously, indicating that the luminescence originates from compound **3a′** (and not an impurity). Only two other examples of axially dissymmetric Pt_2-containing complex [ClPt(μ-dppm)$_2$PtL]$^+$ (L = (4-chlorophenyl)(4-pyridyl)acetylene, λ_{max} = 420 nm, τ_e = 0.21 μs, Φ_e = 0.0071 and *L* = 2,4,6-trimethylpyridine, λ_{max} = 591 nm, τ_e = 3.2 μs)[35,36] were previously reported to be emitting. The nature of the lowest-energy excited state responsible for the emission was assigned to an intraligand $^3\pi\pi^*$ state,[35] while for the second, it was assigned to a ^{3}dσdσ^* state.[36] The spectral and photophysical characteristics are as follows: λ_{max} = 680 nm, τ_e = 6.43 ± 0.1 μs, Φ =

(34) Rashidi, M.; Vittal, J. J.; Puddephatt, R. J. *J. Chem. Soc., Dalton Trans.* **1994**, 1283–1289.
(35) Yip, H.-K.; Che, C.-M.; Peng, S.-M. *J. Chem. Soc.; Dalton Trans.* **1993**, 179–187.

Table 5. Photophysical Data for **3a′** and **8** at 77 K

compounds	solvent used	λ_{em}(nm)	τ (μs)	ϕ
3a′	2-MeTHF	630	12.7 ± 0.467	*a*
	PrCN	680	6.43 ± 0.1	0.0033
	solid	690		
8	PrCN	730	*a*	*b*

[a] Not measured. [b] Too weak to be measured accurately.

0.0033 (Table 5). These values compare very favorably with the data reported earlier for the $[(RNC)Pt(\mu\text{-dppm})_2Pt(CNR)]^{2+}$ complexes (R = *p*-C_6H_4*i*Pr, *t*Bu).[5]

The absorption spectrum of **3a′** (Figure 5) exhibits a shoulder at about 350 nm (in acetonitrile; ε = 4500 M^{-1} cm^{-1}) and lower at 77 K in butyronitrile (~360 nm), which sharpens sensitively upon cooling. This band cannot readily be assigned to the d$\sigma\rightarrow$dσ* transition typical for d^9-d^9 M_2-bonded complexes since the absorptivity is somewhat too low.[5] Something more is occurring.

In order to address this feature, DFT and TDDFT are used. Since the X-ray structures are not always available, geometry optimization was performed on the selected complexes. Prior to analysis, the methodology was tested using the crystallographically characterized complex $[(t\text{BuNC})Pt(\mu\text{-dppm})_2Pt(CNt\text{Bu})]^{2+}$ containing a M−M bond,[5] and the detail of the comparison is placed in the Supporting Information. The reason for this choice stems from the lower-quality data set of complex **3a′**. On average, the Pt−C (X-ray ~1.98 Å), Pt−P (X-ray ~2.28 Å), and Pt−Pt (X-ray ~ 2.64 Å) bond lengths are computed to be 0.05, 0.06, and 0.07 Å longer than the those in the experimental data, representing a lengthening of ~2.5, ~2.6, and ~2.7%, respectively. We find this comparison reasonable. Results for geometry optimization for the complexes **3b**, **4b**, **11a**, and **11b** are presented in Scheme 6. The comparison of the computed structural parameters with the X-ray data, notably for complexes **4b** and **11b**, is similar to that described above, except that the M−X bonds are calculated to be 0.1 Å longer than those in the X-ray data, representing a difference of 4 (Pt−Cl) and 3.8% (Pd−I). The comparison of the MO schemes and TDDFT results is made on the basis of the optimized geometry computations for reasons of homogeneity.

The MO picture of the frontier MOs of compound **3b** is shown in Figure 6. It is reasonably assumed that the conclusions drawn from this analysis are transferable to the other d^9-d^9 species in this work, notably to the mixed-metal Pd−Pt systems. This assumption is based upon the resemblance of the UV−vis spectra of $[ClPt(\mu\text{-dppm})_2PtCl]$ and $[ClPd(\mu\text{-dppm})_2PtCl]$. Moreover, the computations were performed on compound **3b** only. In this case, the arylisocyanide group bears an isopropyl substituent. It is assumed that the conclusions drawn from these calculations can also be transposed to the case where the aryl group is modified by substitution (e.g., xylyl and anisyl, for example). Again, the argument is based on the resemblance of the UV−visible spectra. The HOMO and HOMO−1 of **3b** are composed of the Pt(d_{xz})−Cl(p_x) and Pt(d_{yz})−Cl(p_y) components, where a minor contribution is computed on the Pt atom that binds the CNR ligand. In other words, for these two MOs, the electronic density is placed primarily on the Pt−Cl fragment. On the basis of symmetry and signs of the orbitals, this MO is the equivalent of a dπ*. The LUMO is a π* orbital of the aromatic-NC system with a minor component on the Pt binding this RNC ligand. This diagram is also composed of two sets of bonding dσ orbitals (HOMO−2 and HOMO−3) built upon Pt($d_{x^2-y^2}$)−Pt(d_z^2) and Pt($d_{x^2-y^2}$)−Pt($d_{x^2-y^2}$) with some bonding and antibonding Pt−Cl(n) interactions, respectively. The LUMO+1 is an antibonding version of the HOMO−3 (i.e., Pt($d_{x^2-y^2}$)−Pt($d_{x^2-y^2}$). On the basis of TDDFT computations, the lowest-energy electronic transition is composed of three major components, HOMO→LUMO, HOMO−2→LUMO+1, and HOMO−3→LUMO+1, with relative weights of 0.57, 0.20, and 0.31, respectively. The former transition is a metal/halide-to-ligand charger-transfer (M/XLCT) process from the Pt−Cl fragment to the π* RNC component, and the two latter ones are the dσ−dσ* ones expected for the M_2-bonded species. All in all, the lowest-energy electronic transition is a mixture of M/XLCT and

Scheme 6. Geometry Optimization by DFT (P = PPh_2)

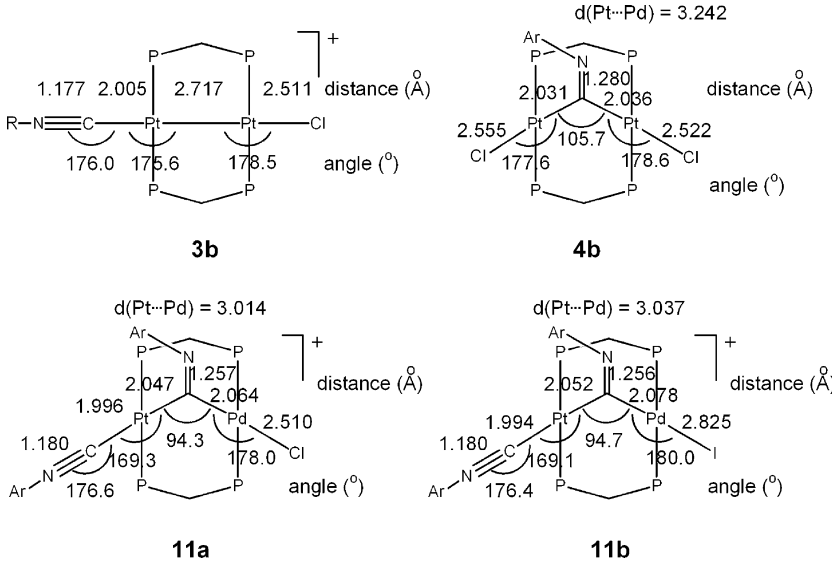

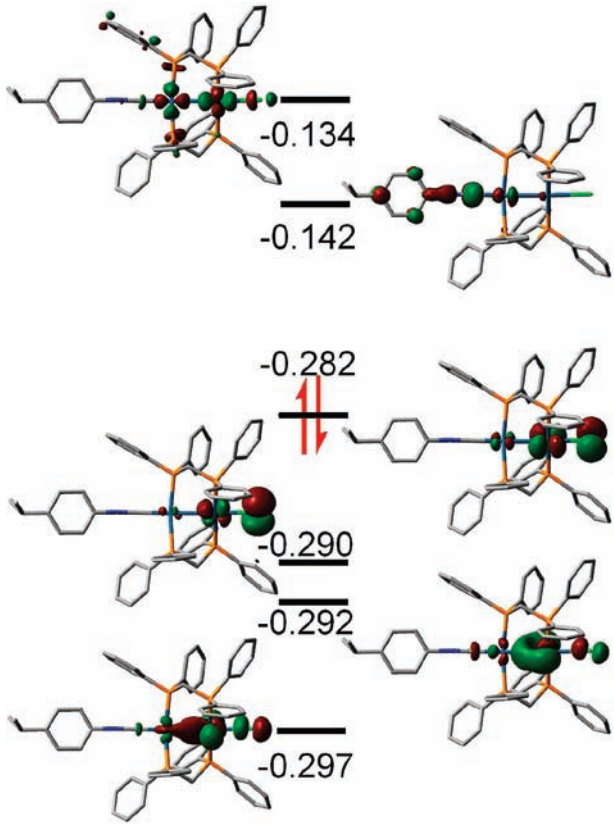

Figure 6. MO pictures of the frontier MOs of complex **3b**. The MO energies are in au units.

dσ−dσ*. The computed oscillator strength is 0.053, consistent with the reported modest absorptivity, and may be a consequence of the fact that the two contributing electronic transitions are polarized along two different axes as well as the presence of a dihedral angle of about 35°. The computed position of this band is 387 nm when all three components are used. Using simply the HOMO−LUMO gap, we compute 326 nm (Figure 6). Both values, 326 and 387 nm, are in the same range as the experimental value (355 at room temperature and 360 at 77 K).

At room temperature, the luminescence for **3a′** is not detectable in fluid solution (PrCN) and is weak in the solid state (not enough to extract τ_e) but exhibits about the same emission maximum. In this respect, compound **3a′** behaves the same way as compounds **16** and **17**, for which emission lifetimes were measured.[5] Compound **8** is also interesting since it exhibits a head-to-tail structure where the P donor coordinates the Pt center and the RNC ligand occupies the remaining Pd metal. This preferential site occupancy is based on the observation that the P atom also coordinates the Pt atom in **7**, potentially leading to the synthesis of head-to-tail organometallic and coordination polymers using dissymmetric bidentate assembling ligand. The heterobinuclear complex **8** exhibits a strikingly similar spectrum to that of **3a′** (Figure 7), allowing us to make the assignment for the observed band at 365 nm the same transition, that is, M/XLCT-dσ→dσ* with M = Pt and X = P.

Compound **8** is also luminescent, as this was the case for compounds **3a′** and **3b**. It exhibits similar features to those of the homobinuclear complex **3a′** (unresolved band, λ_{max} at

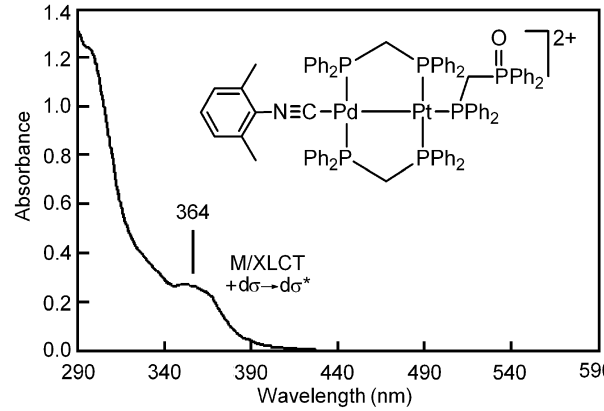

Figure 7. Absorption spectra of **8** in PrCN at 77 K.

about 730 nm). Unfortunately, the harmonic of the excitation light cluttered the emission band, so the photophysical data could not be extracted. The fact that no vibronic structure is observed in the emission band strongly suggests that the emission does not arise from an intraligand $\pi\pi$* state. Since the emission maximum compares favorably to that reported for $Pd_2(dppm)_2(CNtBu)_2^{2+}$ (730 nm) and **3a′** (680 nm, PrCN), we propose to assign the lowest energy-emitting excited state as M/XLCT-dσ→dσ* as well. Moreover, the emission lifetimes (microsecond time scale; see Table 5) and the large energy gap between the absorption and the emission (Stoke shift, ∼12 000 cm^{-1}) strongly suggest that the emission arises from a triplet state, totally consistent with the presence of heavy metals.

No emission was observed at room temperature for **3a′** and **8** in fluid solution, which is consistent with the known facile photoinduced M−M bond cleavage in d^9−d^9 species. In the solid state, a very weak emission centered at about the same position was observed, but the intensity was too weak to be exploited. This phenomenon is not uncommon for such Pd-containing d^9−d^9 complexes.[5]

We attempted to compute the position of the emission band of **3b**. First, the geometry of **3b** in its triplet state was optimized in order to extract the corresponding MO energies, notably that of the highest semi-occupied molecular orbital (HSOMO). Unfortunately, the geometry distorted drastically where M−M and M−X bond dissociations were computed, and strong angle deviations were noted. In other words, the weakening of these bonds upon the dσ→dσ* transition induced a far too large excited-state distortion to render this technique exploitable. This is consistent with the fact that absence of emission is often noted for these complexes notably in fluid solution at room temperature. In the solid state or in frozen matrices, emission is observed, indicating that, indeed, the matrix prevents major excited-state distortion since the chromophore is trapped inside a rigid matrix. In such a case, the ground-state geometry was used to compute the HSOMO in the triplet state. For **3b**, this energy gap was −0.171 au, and a value of 414 nm was computed for the position of the triplet emission. The conclusion is that some excited-state distortion must occur, but we do not know a

Table 6. Photophysical Data for d^8-d^8 A-Frame Homo- and Heterobimetallic Systems **4b**, **9**, **11a**, **11b** at 77 K

compounds	solvent used	λ_{em}(nm)[a]	τ (μs)	ϕ
4b	2-MeTHF	625	15.7 ± 0.13	*b*
	PrCN	625	8.6 ± 0.13	0.013
	solid	620	*b*	*b*
9	2-MeTHF	650	0.897 ± 0.01	*b*
	PrCN	700	0.516 ± 0.023	0.0027
	solid	740	*b*	*b*
11a	2-MeTHF	660	12.04 ± 1.029	*b*
	PrCN	710	3.06 ± 0.044	0.0079
11b	2-MeTHF	670	22 ± 1.64	*b*
	PrCN	715	12.7 ± 1.12	0.0043

[a] The large red shift of the emission band and decrease in τ_e by changing the solvent from 2-MeTHF to PrCN could very likely be associated with a halide dissociation in solution and its replacement by the nitrile. [b] Not measured.

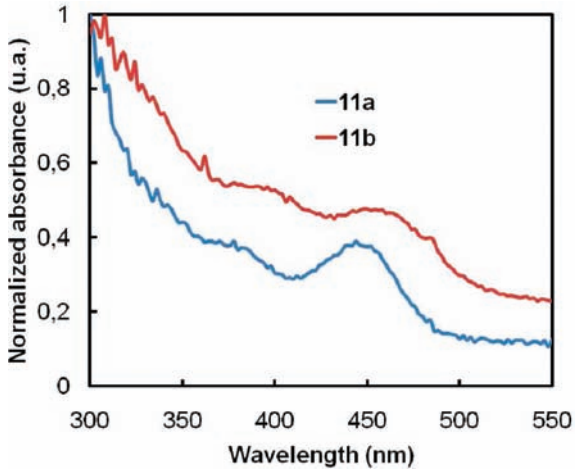

Figure 8. Absorption spectra of **11a** and **11b** in PrCN at 77 K.

way of finding out since it depends on the matrix that keeps the complex together. All in all, this methodology cannot be applied for this complex.

3.2. Photophysical Properties of the d^8-d^8 A-Frame Homo- and Heterobimetallic Systems. Luminescent A-frame complexes are extremely rare. The few known examples include ethynyl-containing d^8-d^8 species and an A-frame triangular Pt_2Au cluster.[37] While compound **10** is not luminescent, compounds **11a** and **11b** are at 77 K in PrCN. The characteristics of these emissions are listed in Table 6. The absorption spectra of **11a** and **11b** exhibit low-energy bands (more red-shifted than that the d^9-d^9 M_2-bonded species discussed above), which are also better resolved at 77 K in the 400−500 nm range (Figure 8).

Isocyanide insertion into the M−M leads to a breakdown of the M−M bond and to a considerable elongation of the M···M interaction (d(Pd···Pt) = 3.0273(9) Å in **11b**). Consequently, a $d\sigma^* \rightarrow d\sigma$ transition can be excluded. Several studies on d^8-d^8 binuclear complexes assigned this low-energy absorption band to a $d\sigma^* \rightarrow p\sigma$ transition.[38] In this case, maximum wavelength absorption is related to the M−M distance and to the nature of substituents ligated to the metal centers.[38]

Similarly, as analyzed above, the nature of this low-energy absorption is addressed by means of DFT and TDDFT. Figure 9 presents the pictures of the relevant frontier MOs of **11a** and **11b**, as computed by DFT. The HOMO and LUMO exhibit complex atomic contributions. In both cases, the HOMO is composed of in-plane atomic contributions: the X(n) donor orbital interacting in an antibonding fashion with the Pd($d_{x^2-y^2}$) orbital, which interacts in a bonding fashion with one of the sp^2-hybridized n orbitals of the C bridging atom, which interacts also in a bonding manner with the Pt($d_{x^2-y^2}$) one. This HOMO is also composed of the N(n) orbital. Very minor contributions of the in-plane NC π^* system are also computed. The major contributions are represented in a simple drawing in Scheme 7.

The LUMO (again in **11a** and **11b**) also exhibits a rather complex series of atomic contributions. The contribution from the halide atom and the μ-CNR is now very small. The nature of the atomic contribution of the Pt atom is now primarily d_{z^2}, and the electronic density on the CN π^* system has significantly augmented. Some modest contributions of

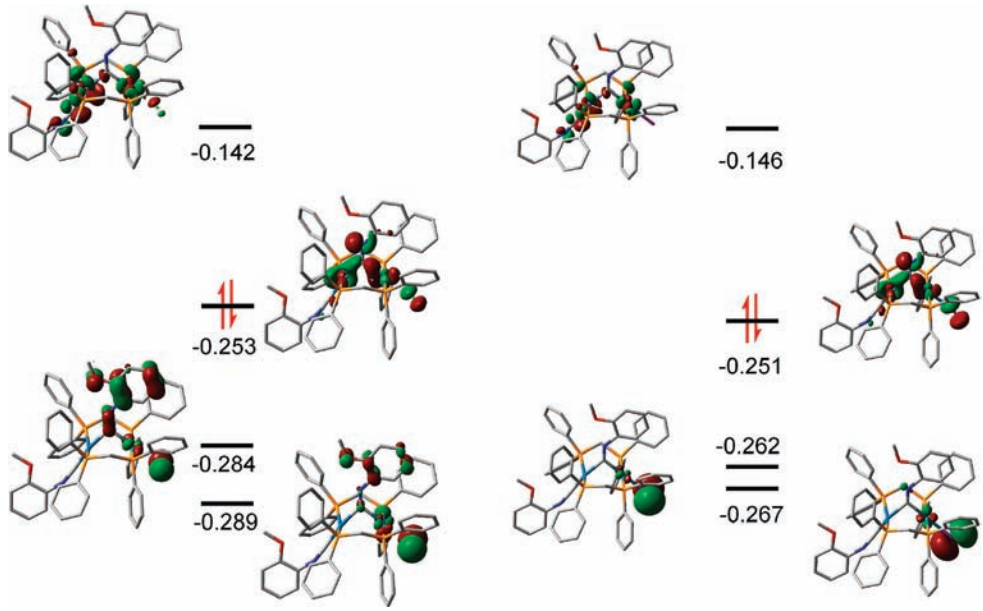

Figure 9. MO pictures of the LUMO, HOMO, HOMO−1, and HOMO−2 of **11a** (right) and **11b** (left).

Scheme 7

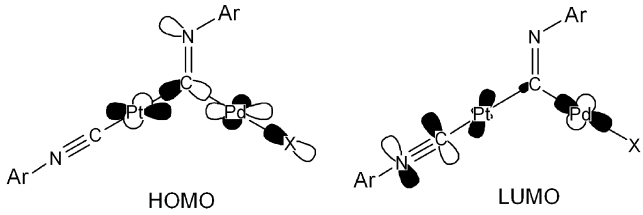

the perpendicular P atoms are also computed and interact with the Pt metal orbital in an antibonding fashion. The HOMO−LUMO transitions are essentially a charge transfer from the Pd/X center and μ-CNR to the terminal RNC π^* system. TDDFT computes that the lowest-energy electronic transition is primarily the expected HOMO→LUMO for both complexes. This computational conclusion comes from the fact that both MOs are well isolated from other frontier MOs, so little mixing occurs. The computed positions for this transition by TDDFT are 496 and 519 nm, whereas the values calculated from the HOMO and LUMO DFT energies are 411 and 434 nm (Scheme 7), for **11a** and **11b**, respectively. Experimentally, the positions for these lower-energy features are seen at 448 and 455 nm, respectively, which fall in the middle of this window. All in all, this reasonable correspondence between the computation and experimental results provides support for the charge-transfer assignment. It is also interesting to note that both dissymmetric d^9-d^9 M_2-bonded and d^8-d^8 A-frame species exhibit a lowest-energy charge-transfer character from the Pd moiety to the RNC−Pt-containing fragment. For the A-frame complexes, computations indicate that this process passes through the central μ-CNR bridge.

Emission spectra in frozen butyronitrile (Figure 10) lead to a broad unstructured band at $\lambda_{max} = 710$ nm ($\tau_e = 3.06 \pm 0.044$ μs, $\phi = 0.0079$) for **11a** and at $\lambda_{max} = 715$ nm ($\tau_e = 12.7 \pm 1.1$ μs, $\phi = 0.0043$) for **11b**. These values are comparable with other A-frame d^8-d^8 systems based on iridium and platinum metal centers.[37a,c] The λ_{max} and the nonradiative deactivation values of dinuclear complexes **11a** and **11b** are in the order **11a** < **11b**, indicating that the nature of the excited states is influenced by the nature of the halide. This behavior has already been observed in other d^8-d^8 homo- and heterobimetallic A-frame polymers[39] and is totally consistent with the change in HOMO−LUMO gap computed by DFT (Figure 9), where this gap is smaller for **11b** (X = I) versus **11a** (X = Cl).

The pseudosymmetric A-frame complex **4b** (considering the fluxion motion of the μ-CNR ligand) is also found to be

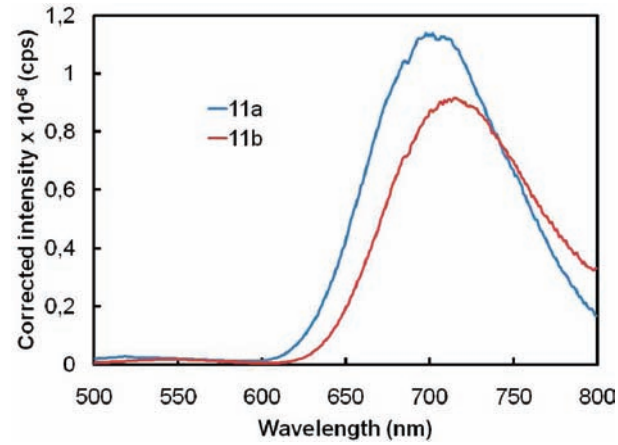

Figure 10. Emission spectra of **11a** (blue) and **11b** (red) in PrCN at 77 K. $\lambda_{exc} = 350$ nm.

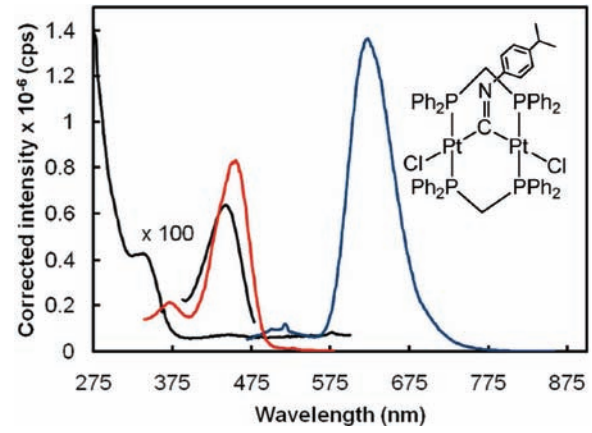

Figure 11. Absorption (black), excitation (red), and emission spectra (blue) of **4b** in PrCN at 77 K. $\lambda_{exc} = 440$ nm.

luminescent at 77 K (Figure 11). Its absorption spectrum is characterized by an absorption band at ~350 nm, and a weaker feature at ~440 nm. The excitation spectrum (in red) overlaps with the absorption, again illustrating that the observed emission does not arise from an impurity. This comparison is important because it refers to the equilibrium between the two species illustrated in Scheme 4 between the d^8-d^8 A-frame neutral species **4b** and the d^9-d^9 M_2-bonded chloride salt, **3b**. Upon cooling, the equilibrium shifted toward the neutral species, preventing ligand dissociation, but this does not necessarily preclude the possibility of having traces of the d^9-d^9 M_2-bonded complex. In this work, we had no spectroscopic evidence for this species, as both the absorption and emission spectra are different from that of **3a′** above.

The analysis of the absorption spectrum was addressed in a similar manner to that illustrated above. The picture of selected relevant MOs of **4b** is presented in Figure 12. The HOMO is composed of Pt($d_{x^2-y^2}$) in bonding interactions with the in-plane μ-C(n) and in antibonding interactions with the in-plane Cl(n). In-plane N(n) contribution is also computed, which overall makes this MO bear a very close resemblance to the corresponding HOMOs of **11a** and **11b** (Figure 9 and Scheme 7). The presence of a bent static structure of the μ-CNR group does not affect the relative amplitude of the atomic contributions on the right- and left-hand sides. We

(36) Hong, X.; Yip, H.-K.; Cheung, K.-K.; Che, C.-M. *J. Chem. Soc., Dalton Trans.* **1993**, 815–816.
(37) (a) Marshall, J. L.; Hopkins, M. D.; Miskowski, V. M.; Gray, H. B. *Inorg. Chem.* **1992**, *31*, 5034–5040. (b) Balch, A. L. *J. Am. Chem. Soc.* **1976**, *98*, 8049–8054. (c) Che, C. M.; Yam, V. W.-W.; Wong, W.-T.; Lai, T. F. *Inorg. Chem.* **1989**, *28*, 2908–2910.
(38) (a) Sacksteder, L.; Baralt, E.; DeGraff, B. A.; Lukehart, C. M.; Demas, J. N. *Inorg. Chem.* **1991**, *30*, 3955–3957. (b) Nieuwenhuis, H. A.; Stufkens, D. J.; Vicek, A., Jr. *Inorg. Chem.* **1995**, *34*, 3879–3886.
(39) Synthesis, characterization, photophysical properties of these polymeric systems are described and published elsewhere: Clément, S.; Aly, S. M.; Husson, J.; Fortin, D.; Strohmann, C.; Knorr, M.; Guyard, L.; Abd-El-Aziz, A. S.; D. Harvey, P. D. *Eur. J. Inorg. Chem.* **2009**, in press.

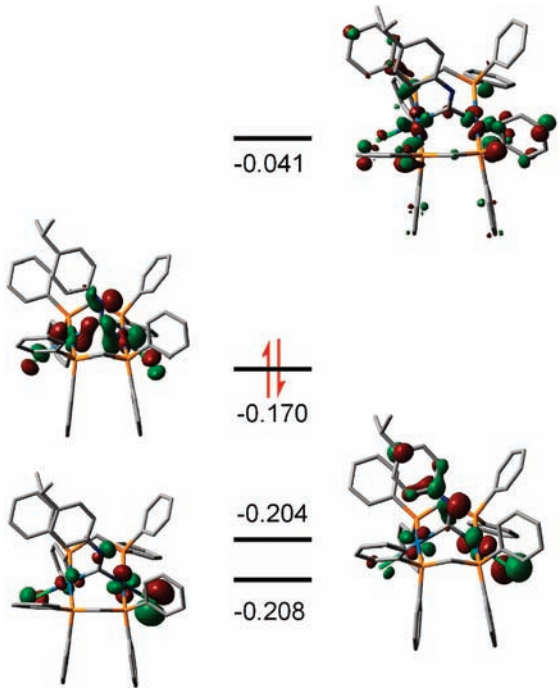

Figure 12. MO pictures of the LUMO, HOMO, HOMO−1, and HOMO−2 of **4b**.

can almost assess this MO as having a mirror plane on the μ-C═N axis. The LUMO is composed of Pt($d_{x^2-y^2}$) and a minor contribution of in-plane Cl(n), but also of P(n) and some phenyl π^* orbitals of both the dppm and RNC ligand. An electronic transition between the HOMO and the LUMO would lead to a change in electronic density mostly located in-plane, primarily on the Cl−Pt−C−Pt−Cl bent frame to both almost perpendicularly placed P−Pt−P axes, reflecting the typical d−d transition in square-planar complexes. This quasi-perpendicular orientation of the electronic density shift upon excitation suggests a lower overlap between the two sets of orbitals. All in all, this means that this specific transition would have a low probability.

TDDFT computes that the lowest-energy electronic transition is indeed the expected HOMO−LUMO process with a minor component of HOMO−LUMO+1. The relative contributions of these two processes are 0.65 and 0.11, respectively, so the second process is not analyzed here. The position computed by TDDFT for this transition is 419 nm, not too far away from the experimental value of 440 nm (Figure 11). The HOMO−LUMO gap computed by DFT is 348 nm, a value that we consider far. The problem is that the molecule must exhibit a large excited-state distortion that is not taken into account in the computations. The modest computed oscillator strength (0.15) is also consistent with the observable low absorptivity (Figure 11). We could not reliably calculate the experimental absorptivity value because of the presence of two species in solution, as illustrated in Scheme 4.

TDDFT coupled with DFT computations were also performed in order to address the observed emission at ∼625 nm (Figure 11). Again, because of the large energy gap between the absorption and emission (∼7000 cm^{-1}) and the long emission lifetime (microsecond time scale), this luminescence is assigned to phosphorescence. We encountered similar problems when attempting to optimize the geometry of **4b** in its triplet state. Pt−Cl bond dissociation was calculated, and we could not address reliably the HSOMO energy. On the other hand, by keeping the ground-state structure for the triplet state calculations, which obviously does not represent the real situation here but is used as an approximation, a HSOMO energy of −0.079 au is computed. This MO level is placed ∼0.093 au above the HOMO of **4b** (Figure 12), which would place the position of the phosphorescence at 490 nm. This value is strongly blue-shifted with respect to the observed maximum (625 nm). By considering that this methodology of estimating the position of an emission from the HOMO−LUMO gap always provides blue-shifted estimated values (see above), the this 490 nm value is not surprising. We propose that the observed emission at 625 nm arises from a quasi d−d state, as discussed above where the metal center is the Pt···Pt unit and the sets of ligands are the Cl's and μ-CN on one hand and the perpendicular P's on the other.

In the solid state, a very weak emission centered at about the same position as described below was observed for **4b**, **9**, **11a**, and **11b**, but the intensity was too weak to be exploited. All photophysical data obtained for d^9−d^9 homo- and heterobimetallic systems are summarized in Table 6.

Conclusion

This study provides a better understanding of coordination properties for various CNR ligands in homo- and heterodinuclear M−M bonded complexes, in particular, of what controls the bridging versus terminal coordination mode. Various subtle parameters influence the coordination mode: (i) the π-acceptor propensity of the isocyanide ligand, (ii) the nature of the M−X bond, and finally, (iii) the polarity of the solvent. In the case of a bridging coordination, the bending of the μ-CNR ligand is generally observed, allowing the control of the electronic density on metal centers by backbonding. These findings help us to select the appropriate assembling diisocyanide ligands to promote A-frame-containing coordination polymers, avoiding the undesired halide ligand dissociation. This would help us in addressing the structure at all times.

We also find that the investigated complexes, which are used as model compounds for the A-frame-containing polymers, notably for complexes **11a** and **11b**, are most currently modestly luminescent at 77 K in both the solid state and in solution, leading to unstructured emission bands in the 600−800 nm window. At the same time, this work provides an insight into the nature of the luminescence in both the dissymmetric M_2-bonded chromophores and the A-frame species. M/XLCT-dσ→dσ^* excited states are predicted for the M_2-bonded complexes, and M/XLCT-states are also concluded for the A-frame species, in particular for compounds **11a** and **11b**, on the basis of DFT/TDDFT computations. The preparation and photophysical characterization of a series of corresponding

A-frame-containing polymers are underway and will be reported shortly.[39]

Acknowledgment. P.D.H. thanks the Natural Sciences and Engineering Research Council of Canada (NSERC), the Fonds Québécois sur la Recherche des Sciences de la Nature et des Technologies (FQRNT) for a postdoctoral fellowship for S.C., and the Centre d'Études sur les Matériaux Optiques et Photoniques de l'Université de Sherbrooke (CEMOPUS) for funding. M.K. thanks the French Ministère de la Recherche et de la Technologie for financial support and a Ph.D. grant for S.C.

Supporting Information Available: ^{31}P NMR spectrum of **8** in $CDCl_3$. X-ray structure of **3a′**. Absorption, excitation and emission spectra in fluid solution at 77 K of **3a′**, **4b**, **11a**, and **11b**. Solid-state emission spectra of **4b** at 77 K. Comparison between the computed structure of $[Pt_2(dppm)_2(CN\textit{t}Bu)_2]^{2+}$ (DFT) and the experimental X-ray data from ref 5. Colored ball-and-stick plots of **4b**, **11b**, and **12**. ^{195}Pt NMR spectrum of **11a** in $CDCl_3$. This material is available free of charge via the Internet at http://pubs.acs.org.

IC8023315